

2009

Improving mid-frequency contrast in sparse aperture optical imaging systems based upon the Golay-N family of arrays

Andrew James Stokes
University of Dayton

Follow this and additional works at: https://ecommons.udayton.edu/graduate_theses

Recommended Citation

Stokes, Andrew James, "Improving mid-frequency contrast in sparse aperture optical imaging systems based upon the Golay-N family of arrays" (2009). *Graduate Theses and Dissertations*. 5814.
https://ecommons.udayton.edu/graduate_theses/5814

This Thesis is brought to you for free and open access by the Theses and Dissertations at eCommons. It has been accepted for inclusion in Graduate Theses and Dissertations by an authorized administrator of eCommons. For more information, please contact mschlangen1@udayton.edu, ecommons@udayton.edu.

**IMPROVING MID-FREQUENCY CONTRAST IN SPARSE
APERTURE OPTICAL IMAGING SYSTEMS BASED
UPON THE GOLAY- N FAMILY OF ARRAYS**

Thesis

Submitted to

The School of Engineering of the

UNIVERSITY OF DAYTON

in Partial Fulfillment of the Requirements for

The Degree

Master of Science in Electro-Optics

by

Andrew James Stokes

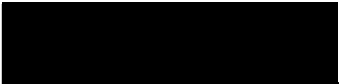
UNIVERSITY OF DAYTON

Dayton, Ohio

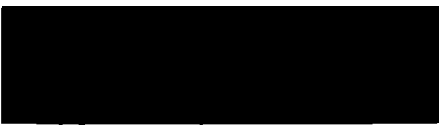
December 2009

**IMPROVING MID-FREQUENCY CONTRAST IN SPARSE
APERTURE OPTICAL IMAGING SYSTEMS BASED UPON THE
GOLAY-N FAMILY OF ARRAYS**

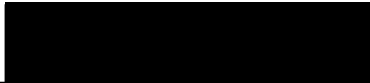
APPROVED BY:




Bradley D. Duncan, Ph.D.
Professor,
Electro-Optics Program
University of Dayton
Committee Chairman




Joseph W. Haus, Ph.D.
Professor and Director,
Electro-Optics Program
University of Dayton
Committee Member



Matthew P. Dierking, Ph.D.
Principal Engineer,
EO Combat ID Branch
Sensors Directorate
Air Force Research Lab
Committee Member



Malcolm W. Daniels, Ph.D.
Associate Dean
School of Engineering



Tony E. Saliba, Ph.D.
Dean
School of Engineering

ABSTRACT

IMPROVING MID-FREQUENCY CONTRAST IN SPARSE APERTURE OPTICAL IMAGING SYSTEMS BASED UPON THE GOLAY- N FAMILY OF ARRAYS

Name: Stokes, Andrew James
University of Dayton

Advisor: Dr. Bradley D. Duncan

Sparse aperture imaging systems are capable of producing high resolution images while maintaining a small overall light collection area compared to a fully filled aperture yielding the same resolution. This is advantageous for applications where size, volume, weight and/or cost are important. However, sparse aperture systems pay the penalty of reduced contrast at midband spatial frequencies. The focus of this work has been on increasing the midband contrast of sparse aperture imaging systems based on the Golay- N family of arrays. These arrays are of interest due to their compact, non-redundant autocorrelations. The modulation transfer function provides a quantitative measure of both the resolution and contrast of an imaging system and, along with an average relative midband contrast metric, will be used to compare perturbations to the Golay arrays. Numerical calculations have been performed to investigate the behavior of Golay-9 and -12 arrays into which autocorrelation redundancy has been introduced. An increase in midband average relative contrast of over 55% was experimentally verified for the Golay-9 array.

ACKNOWLEDGEMENTS

I would like to thank everyone who has provided the opportunity and guidance to complete the scientific research described in this thesis. For providing this opportunity, I am indebted to Robert Feldmann, Chief of the Electro-Optic Combat Identification Technology branch of the Air Force Research Lab, AFRL/RYJM. I would also like to express my sincere appreciation for the time and commitment from my wonderful mentors Dr. Bradley D. Duncan and Dr. Matthew P. Dierking who are my thesis advisor and the technical advisor from AFRL/RYJM, respectively. Drs. Duncan and Dierking have given me not only excellent technical and professional guidance, but have been wonderful life mentors along the way. Also, I would like to thank Nicholas J. Miller of LOCI for being a tremendous help in setting up my laboratory experiment and providing valuable insight to my thesis research.

This effort was supported in part by the U.S. Air Force through contract number FA8650-06-2-1081, and by the Ladar and Optical Communications Institute (LOCI) at the University of Dayton. The views expressed in this article are those of the authors and do not reflect on the official policy of the Air Force, Department of Defense or the U.S. Government.

TABLE OF CONTENTS

ABSTRACT	iii
ACKNOWLEDGEMENTS	iv
LIST OF ILLUSTRATIONS	vii
Chapter 1 INTRODUCTION	1
1.1 Thesis Overview.....	2
Chapter 2 THEORY	4
2.1 Fill Factor (α)	5
2.2 Modulation Transfer Function (MTF).....	6
2.2.1 MTF in an Incoherent, Aberration-free Optical Imaging System	7
2.2.2 Physical Meaning of the MTF.....	9
Chapter 3 GOLAY- <i>N</i> ARRAYS	12
3.1 Golay-3 Array	12
3.2 Golay-6 Array	13
3.3 Golay-9 Array	14
3.4 Golay-12 Array	18
Chapter 4 SPATIAL FREQUENCY AVAILABILITY TECHNIQUE	22
4.1 Calculating the Spatial Frequency Cutoff	23
4.2 Calculating the Midband Average Relative Contrast (ARC).....	25
Chapter 5 INCREASING MIDBAND CONTRAST IN GOLAY-LIKE ARRAYS.....	27
5.1 Introduction of Redundancy	27

5.1.1 Golay-9 Array	27
5.1.2 Golay-12 Array	31
5.2 Discrete Global Apodization Effects, Attenuation.....	34
5.2.1 Golay-9 Array	34
5.2.2 Golay-12 Array	36
Chapter 6 EXPERIMENTAL VERIFICATION OF THEORY	39
6.1 Experimental Setup	39
6.2 Results	40
Chapter 7 SUMMARY AND CONCLUSIONS	42
REFERENCES.....	44

LIST OF ILLUSTRATIONS

Figure 1: Nominal diagrams of the Golay-3, -6, -9 and -12 arrays.....	4
Figure 2: (a) The MTF of a uniform sub-aperture diameter Golay-9 array with $D=2.54\text{mm}$ and $S=1.4$; and (b) a cross-section of (a).	9
Figure 3: (a) The MTF of a uniform sub-aperture diameter Golay-12 array with $S=1.3$; and (b) a cross-section of (a).	10
Figure 4: (a) The MTF of a monolithic aperture nominally achieving the same resolution as the sparse array MTFs seen in Figures 2 and 3; and (b) a cross-section of (a).....	10
Figure 5: Nominal Golay-3 array.	12
Figure 6: Nominal Golay-6 array.	13
Figure 7: Nominal Golay-9 array	14
Figure 8: (a) A uniform sub-aperture diameter Golay-9 array with $D=2.54\text{mm}$ and $S=1.4$; and (b) the MTF generated from (a).....	15
Figure 9: (a) A uniform sub-aperture diameter Golay-9 array with $D=2.54\text{mm}$ and $S=1.4$ with the R_1 set of sub-apertures attenuated by 75%; and (b) the MTF generated from (a).	15
Figure 10: (a) A uniform sub-aperture diameter Golay-9 array with $D=2.54\text{mm}$ and $S=1.4$ with the R_2 set of sub-apertures attenuated by 75%; and (b) the MTF generated from (a).	16
Figure 11: (a) A uniform sub-aperture diameter Golay-9 array with $D=2.54\text{mm}$ and $S=1.4$ with the R_3 set of sub-apertures attenuated by 75%; and (b) the MTF generated from (a).	16
Figure 12: Nominal Golay-12 array.	18
Figure 13: (a) A uniform sub-aperture diameter Golay-12 array with $S=1.3$; and (b) the MTF generated from (a).	19
Figure 14: (a) A uniform sub-aperture diameter Golay-12 array with $S=1.3$ and the R_1 set of sub-apertures attenuated by 75%; and (b) the MTF generated from (a).....	19

Figure 15: (a) A uniform sub-aperture diameter Golay-12 array with $S=1.3$ and the R_{22} set of sub-apertures attenuated by 75%; and (b) the MTF generated from (a).....	20
Figure 16: (a) A uniform sub-aperture diameter Golay-12 array with $S=1.3$ and the R_{21} set of sub-apertures attenuated by 75%; and (b) the MTF generated from (a).....	20
Figure 17: (a) A uniform sub-aperture diameter Golay-12 array with $S=1.3$ and the R_3 set of sub-apertures attenuated by 75%; and (b) the MTF generated from (a).....	21
Figure 18: The MTF of (a) a Golay-9 array with $D=2.54\text{mm}$ and $S=1.4$; and (b) a Golay-12 array with $D=2.54\text{mm}$ and $S=1.3$. The spatial frequency cutoff, determined by the conservative maximum inscribed circle approach, is shown by the white circle.	22
Figure 19: The binary MTF of a Golay-9 array with $S=1.4$ and (a) uniform sub-aperture diameters; and (b) the R_2 sub-aperture diameter increased to 1.6 times the unit diameter.	24
Figure 20: The binary MTF of a Golay-9 array with $S=1.4$ and (a) the R_2 sub-aperture diameter increased to 2.2 times the unit diameter; and (b) the R_2 sub-aperture diameter increased to 2.8 times the unit diameter.	24
Figure 21: Numerical simulations of spatial frequency cutoff ρ_{min} , fill factor α and midband average relative contrast (ARC) for varying D_{R2} with an initial threshold of $T_I=0$ and spatial frequency availability threshold of $T_2=0.98$	28
Figure 22: Numerical simulations of spatial frequency cutoff ρ_{min} , fill factor α and midband average relative contrast (ARC) for varying D_{R2} with an initial threshold of $T_I=0$ and spatial frequency availability threshold of $T_2=0.90$	29
Figure 23: Numerical simulations of spatial frequency cutoff ρ_{min} , fill factor α and midband average relative contrast (ARC) for varying D_{R2} with an initial threshold of $T_I=0.01$ and spatial frequency availability threshold of $T_2=0.98$	29
Figure 24: Numerical simulations of spatial frequency cutoff ρ_{min} , fill factor α and midband average relative contrast (ARC) for varying D_{R2} with an initial threshold of $T_I=0.01$ and spatial frequency availability threshold of $T_2=0.90$	30
Figure 25: Numerical simulations of spatial frequency cutoff ρ_{min} , fill factor α and midband average relative contrast (ARC) for varying D_{R21} with an initial threshold of $T_I=0$ and spatial frequency availability threshold of $T_2=0.98$	31
Figure 26: Numerical simulations of spatial frequency cutoff ρ_{min} , fill factor α and midband average relative contrast (ARC) for varying D_{R21} with an initial threshold of $T_I=0$ and spatial frequency availability threshold of $T_2=0.90$	32
Figure 27: Numerical simulations of spatial frequency cutoff ρ_{min} , fill factor α and midband average relative contrast (ARC) for varying D_{R21} with an initial threshold of $T_I=0.01$ and spatial frequency availability threshold of $T_2=0.98$	32

Figure 28: Numerical simulations of spatial frequency cutoff ρ_{min} , fill factor α and midband average relative contrast (ARC) for varying D_{R2I} with an initial threshold of $T_I=0.01$ and spatial frequency availability threshold of $T_2=0.90$	33
Figure 29: Numerical simulations of midband average relative contrast (ARC) while attenuating the R_3 set of sub-apertures in the uniform sub-aperture diameter Golay-9 array from 50% transmittance to 100% transmittance.	35
Figure 30: Numerical simulations of midband average relative contrast (ARC) while attenuating the R_3 set of sub-apertures in the Golay-9 array with a R_2 sub-aperture diameter of 2.73 times the unit diameter from 50% transmittance to 100% transmittance.	35
Figure 31: Numerical simulations of midband average relative contrast (ARC) while attenuating the R_3 set of sub-apertures in the uniform sub-aperture diameter Golay-12 array from 30% transmittance to 100% transmittance.	37
Figure 32: Numerical simulations of midband average relative contrast (ARC) while attenuating the R_3 set of sub-apertures in the Golay-9 array with a R_{2I} sub-aperture diameter of 2.8 times the unit diameter from 50% transmittance to 100% transmittance.	37
Figure 33: Diagram of the experimental setup.....	40
Figure 34: An example of one set of distinct lobes for which the center-to-center pixel spacing was recorded in (a) the theoretical, unmagnified PSF; and (b) an experimental, magnified PSF.	40
Figure 35: Theoretical (solid) and experimental (dashed) calculations of spatial frequency cutoff ρ_{min} , fill factor α and midband average relative contrast (ARC) using an initial threshold of $T_I=0.01$ and a spatial frequency availability threshold of $T_2=0.98$	41

CHAPTER 1

INTRODUCTION

Sparse aperture imaging systems are capable of producing high resolution images while maintaining an overall light collection area that is small with respect to a fully-filled aperture achieving the same resolution. Such systems have advantages over resolution-equivalent monolithic apertures due to their lower size, weight and volume [1], as well as cost efficiency [2].

The modulation transfer function (MTF) of sparse aperture imaging systems will, in general, have a main lobe whose pass-band (midband) spatial frequencies contain lower energy than a fully-filled aperture with the same spatial frequency cutoff. If the midband frequency content becomes too low, or drops to zero, then all information at the corresponding spatial frequencies will be lost. A sparse array could in theory be tailored on an object-dependant basis such that the pass-band of the system is in the region of interest [3]. However, this is unlikely to be the case for any practical implementation of an imaging system designed for unknown targets.

In general, a quality sparse aperture imaging system will be designed such that the autocorrelation of the aperture function (i.e. the imaging system's pupil) produces an MTF that covers most of the spatial frequencies that a filled aperture would capture [4].

In particular, the Golay arrays are beneficial due to their compact, non-redundant autocorrelations [5], which can nearly uniformly fill spatial frequency space with minimal or no zeros present in the MTF.

Although the Golay family of arrays provide the most uniform coverage in Fourier space, these sparse systems are hindered by reduced midband contrast, which gives rise to signal-to-noise ratio (SNR) difficulties and a lower overall image quality. Solutions to this problem, including using long integration times and sophisticated post processing algorithms have been used [6,7]; however, the purpose of this work has been to increase the midband contrast by using the systematic introduction of redundancy in the aperture array itself and through the attenuation of the outer-most set of sub-apertures. In particular, the focus of this work was to increase the midband contrast of sparse aperture imaging systems based upon the Golay-9, as it has been previously shown that a uniform sub-aperture diameter Golay-9, with an expansion factor of 1.4, can optimally maximize resolution and minimize overall pupil plane collection area while also maintaining acceptable MTF side-lobe levels [8]. Also discussed are the Golay-3 and -6 arrays as well as efforts to enhance the midband contrast of a Golay-12 array.

1.1 Thesis Overview

In Chapter 2, THEORY, the geometry of the Golay family of arrays is presented. Quantitative metrics such as fill factor α and the modulation transfer function (MTF) are presented along with their relevance to theory and experiments. In Chapter 3, GOLAY ARRAYS, the geometry of the Golay family of arrays are presented in detail. Motivation

and explanation of a plan to increase the midband average relative contrast (ARC) in each array. In Chapter 4, SPATIAL FREQUENCY AVAILABILITY TECHNIQUE, the spatial frequency cutoff ρ_{min} of the Golay-9 and -12 arrays is explained and a newly developed algorithm: the spatial frequency availability technique is discussed. Also discussed is a midband average relative contrast metric and how it is used to compare perturbations in the Golay-9 and -12 arrays. In Chapter 5, INCREASING MIDBAND CONTRAST IN GOLAY-LIKE ARRAYS, the numerical expectations of the metrics are presented for the introduction of autocorrelation redundancy by enlarging the intermediate set of sub-apertures in the Golay-9 and -12 arrays. Also presented are the numerical calculations of ARC while the outer-most set of sub-apertures is attenuated. Chapter 6, EXPERIMENTAL VERIFICATION OF THEORY, presents the experimental setup to verify the numerical expectations of fill factor, spatial frequency cutoff and ARC for increased autocorrelation redundancy in the Golay-9 array. The results of this experiment are reported and discussed. Finally, in Chapter 7, SUMMARY AND CONCLUSIONS, an overview and summary of this work is presented.

CHAPTER 2

THEORY

The Golay-3, -6, -9 and -12 arrays consist of sets of three diffraction-limited sub-apertures that lie on unique radii from the center of the array. The geometries of these arrays are shown in Figure 1.

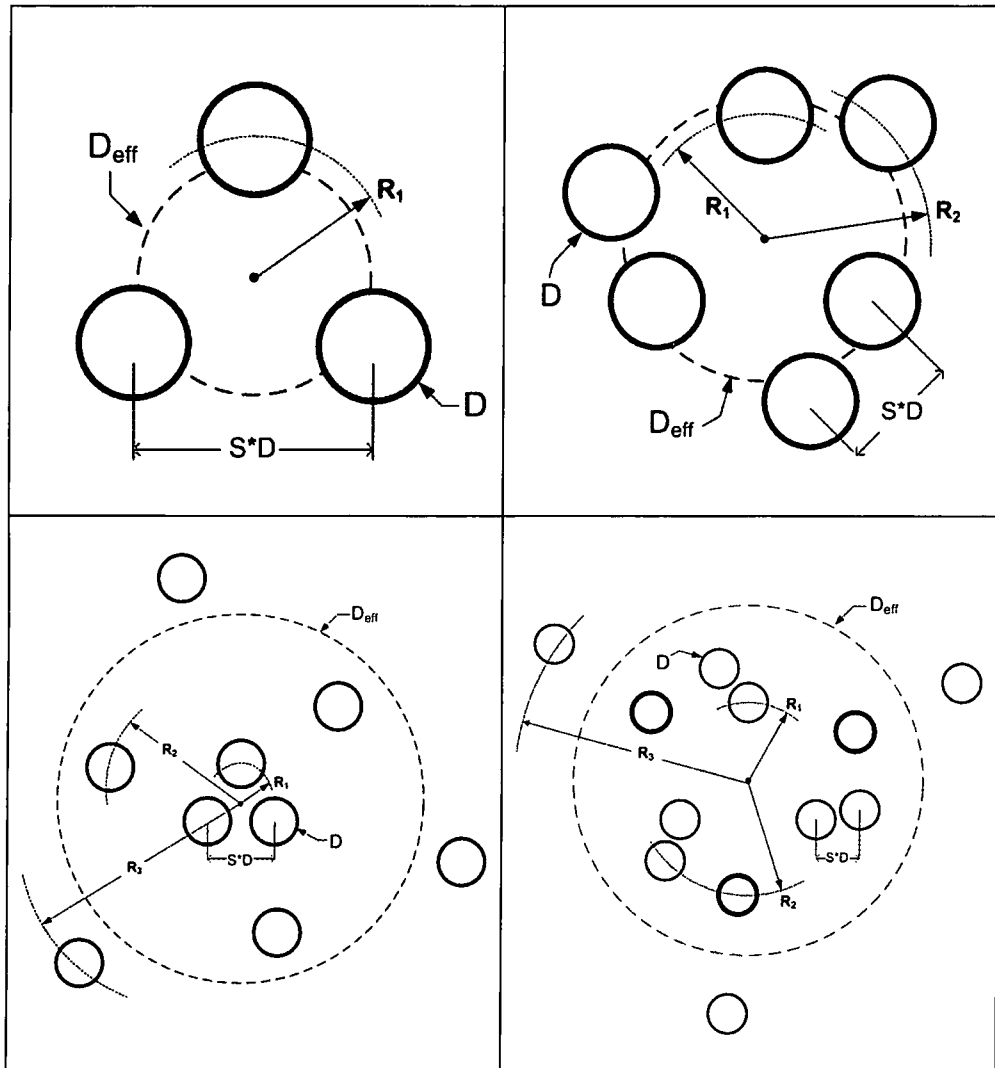


Figure 1: Nominal diagrams of the Golay-3, -6, -9 and -12 arrays.

The inner-most set of sub-apertures lies on the radius R_1 in each of the Golay arrays and each other set of sub-apertures will lie on another unique radius R_n from the center of the array except for the Golay-12 which has two distinct sets of three sub-apertures that lie on a radius R_2 . The center-to-center spacing of the most closely spaced sub-apertures is given by $S \cdot D$ where S is the expansion factor and D is the diameter of the sub-apertures. The nominal effective diameter D_{eff} is shown for each array and its significance will be discussed later in this chapter.

2.1 Fill Factor (α)

An important quantitative performance metric in sparse aperture imaging systems is the fill factor α which is defined as the ratio of the light collection area normalized with respect to the area of a fully-filled aperture capable of achieving the same resolution. The fill factor for a Golay- N array is given by

$$\alpha = \frac{\sum_{n=1}^N 3D_{Rn}^2}{D_{eff}^2}, \quad (1)$$

where n is the common radius number of a set of three sub-apertures and D_{Rn} describes the diameter of the R_n set of sub-apertures. It is important to note that the Golay-12

contains two sets of three sub-apertures that lie on the radius R_2 and therefore the fill factor would become

$$\alpha = \frac{3D_{R1}^2 + 3D_{R21}^2 + 3D_{R22}^2 + 3D_{R3}^2}{D_{eff}^2}, \quad (2)$$

where D_{R21} denotes the highlighted set of sub-apertures located on radius R_2 and D_{R22} denotes the other set of sub-apertures that lie on the radius R_2 .

Recall that the goal of sparse aperture imaging is to achieve resolution comparable to that of a fully-filled monolithic aperture while maintaining a sparse fill factor. A sparse array will then correspond to an effective fully-filled aperture with diameter D_{eff} , related to the spatial frequency cutoff ρ_{min} of the modulation transfer function according to

$$D_{eff} = \rho_{min} \lambda z_i, \quad (3)$$

where λ is the source wavelength and z_i is the distance from the pupil plane to the object, commonly taken to be one focal length.

2.2 Modulation Transfer Function (MTF)

It is well known that the modulation transfer function (MTF) describes an incoherent imaging system's ability to transfer object contrast to an image as a function of spatial frequency [9]. The MTF is preferable for quantifying image quality because it contains

more information of the imaging process than the Rayleigh, Strehl or other single-number measure [10]. This is due to the fact that the MTF is directionally dependant in the spatial frequency plane and contains information specific to resolution *and* image contrast.

2.2.1 MTF in an Incoherent, Aberration-free Optical Imaging System

Using incoherent illumination, the image formed by an imaging system is described by the intensity convolution integral. Furthermore, the normalized transfer function (optical transfer function or OTF) of an aberration-free, incoherent optical imaging system is given by

$$OTF(f_x, f_y) = \frac{\int_{-\infty}^{\infty} \int_{-\infty}^{\infty} |h(u, v)|^2 \exp[-j2\pi(f_x u + f_y v)] du dv}{\int_{-\infty}^{\infty} \int_{-\infty}^{\infty} |h(u, v)|^2 du dv}, \quad (4)$$

where $|h(u, v)|^2$ is the intensity point spread function (PSF) of the optical system, $f_x = x/\lambda z_i$, $f_y = y/\lambda z_i$, x and y are spatial variables [9]. The OTF is simply the normalized 2-dimensional spatial Fourier transform of the intensity PSF.

With the use of Parseval's theorem and the change of variables we arrive at the normalized autocorrelation function given by

$$OTF(f_x, f_y) = \frac{\int_{-\infty}^{\infty} \int_{-\infty}^{\infty} H\left(p + \frac{f_x}{2}, q + \frac{f_y}{2}\right) H^*\left(p - \frac{f_x}{2}, q - \frac{f_y}{2}\right) dp dq}{\int_{-\infty}^{\infty} \int_{-\infty}^{\infty} |H(p, q)|^2 dp dq}, \quad (5)$$

where H is the amplitude transfer function given by $H = \mathfrak{F}\{h\}$ and p and q are integration variables with the same units as f_x and f_y [9].

For a diffraction-limited, aberration-free optical imaging system, the amplitude transfer function is the scaled pupil function, i.e. $H(f_x, f_y) = P(\lambda z_i f_x, \lambda z_i f_y)$. Furthermore, since the system is aberration free, the transfer function will be real-valued and therefore $H^*(f_x, f_y) = H(f_x, f_y)$. Then, using a change of variables the optical transfer function becomes

$$OTF(f_x, f_y) = \frac{\int_{-\infty}^{\infty} \int_{-\infty}^{\infty} P\left(x + \frac{\lambda z_i f_x}{2}, y + \frac{\lambda z_i f_y}{2}\right) P\left(x - \frac{\lambda z_i f_x}{2}, y - \frac{\lambda z_i f_y}{2}\right) dx dy}{\int_{-\infty}^{\infty} \int_{-\infty}^{\infty} P(x, y) dx dy}, \quad (6)$$

which is simply the normalized autocorrelation of the pupil [9]. Note that equation (6) is normalized by the spatial integration of the pupil, not the pupil squared because the aberration-free pupil function is assumed to be binary. Furthermore, the modulation transfer function is simply the modulus of the OTF.

2.2.2 Physical Meaning of the MTF

The MTF is a useful metric in that it contains information about the resolution and optical power, which is a measure of contrast, of an imaging system and is direction-dependant in the spatial frequency domain. Example MTFs are presented below for a uniform sub-aperture diameter Golay-9 array with an expansion factor of 1.4 and a Golay-12 with an expansion factor of 1.3 along with the MTF produced from a nominally resolution-equivalent monolithic aperture. Note that a uniform diameter Golay-9 array with an expansion factor of 1.4 has previously been shown to maximize resolution and minimize overall pupil plane collection area while maintaining acceptable MTF side-band levels and an expansion factor of 1.3 for the uniform sub-aperture diameter Golay-12 was shown to be optimum for its geometry [8].

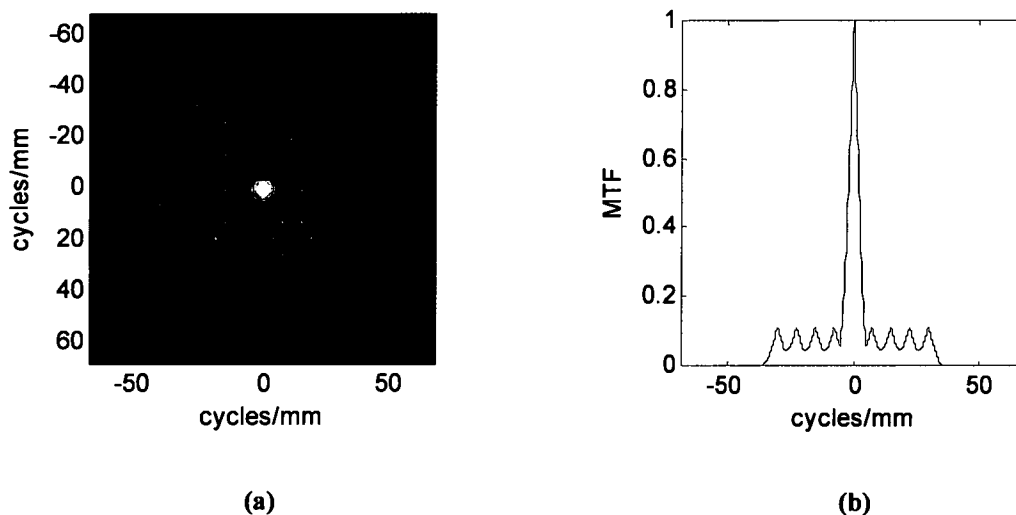


Figure 2: (a) The MTF of a uniform sub-aperture diameter Golay-9 array with $D=2.54\text{mm}$ and $S=1.4$; and (b) a cross-section of (a).

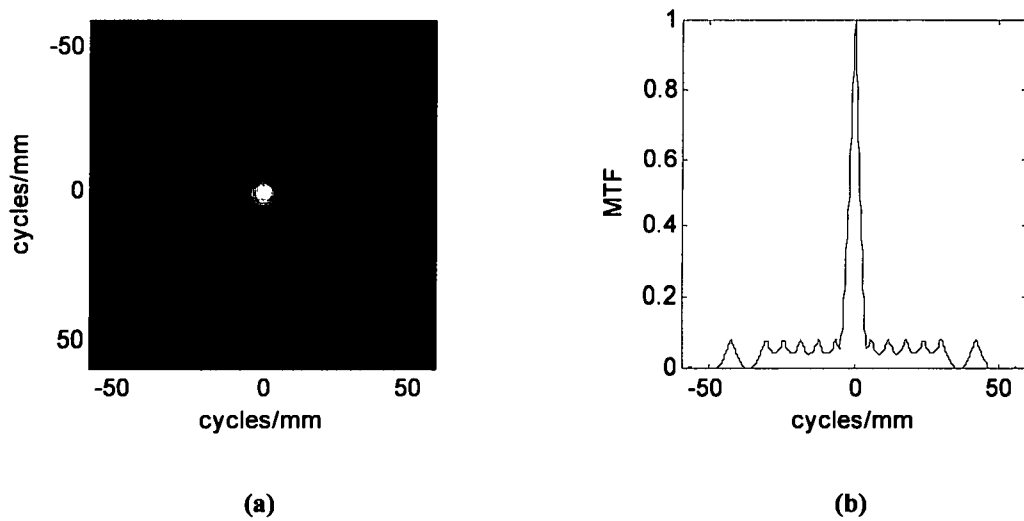


Figure 3: (a) The MTF of a uniform sub-aperture diameter Golay-12 array with $S=1.3$; and (b) a cross-section of (a).

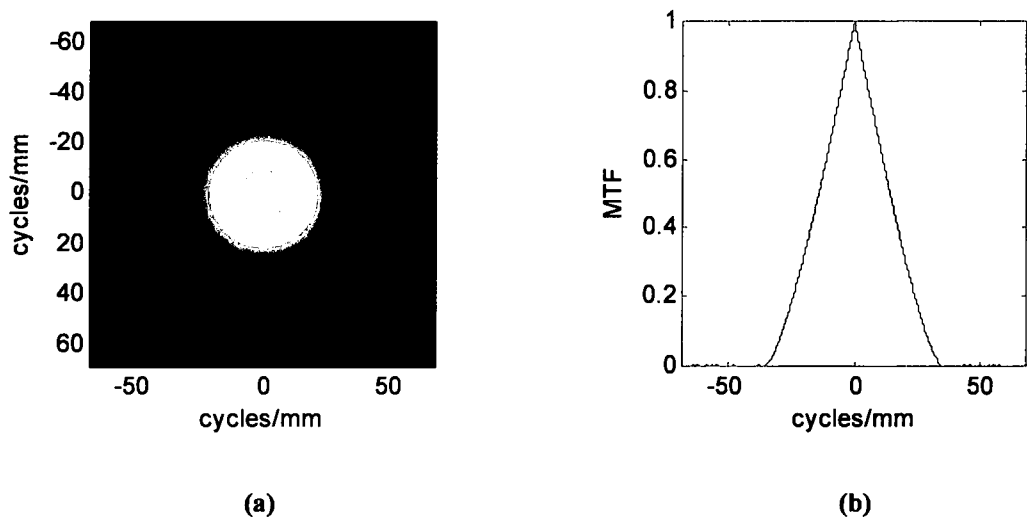


Figure 4: (a) The MTF of a monolithic aperture nominally achieving the same resolution as the sparse array MTFs seen in Figures 2 and 3; and (b) a cross-section of (a).

Recalling that MTF level is a measure of contrast, it is easy to see from Figures 2-4 that the sparse arrays suffers from reduced MTF levels, in particular the midband contrast.

Nominally speaking, the spatial frequency cutoff (i.e. resolution) is where the MTF drops to zero; however, the subtleties of determining the spatial frequency cutoff of the MTF of a sparse array will be discussed in detail in Chapter 4.

It is important to note that regarding the OTF as the normalized autocorrelation of the pupil provides intuitive insight; however, equation (4) will be used to calculate the OTF of the experimental imaging system. Specifically, a CCD array will record the intensity point spread function $|h(u, v)|^2$, which is Fourier transformed and normalized. Finally, the MTF is obtained by taking the modulus of that result.

CHAPTER 3

GOLAY-N ARRAYS

3.1 Golay-3 Array

The Golay-3 array consists of one set of three sub-apertures which lie on the same radius R_1 from the center of the array, as seen in Figure 5.

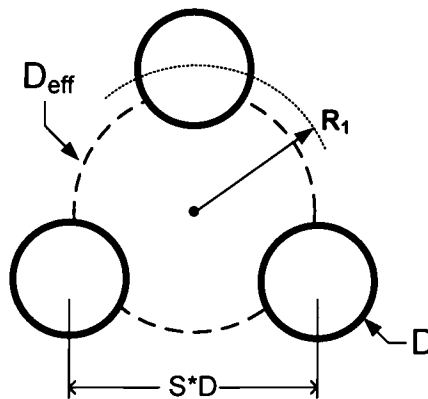


Figure 5: Nominal Golay-3 array.

The MTF generated from a Golay-3 consists of a normalized main lobe and smaller side-lobes, similar to Figures (2) and (3). If the expansion factor were to be increased beyond the optimum of $S=1.6$, holes/nulls would become present in the MTF [8]. Moreover, increasing the expansion factor will not add or boost any MTF information in the desired mid-spatial frequency region and therefore will not be an option in altering these arrays.

Then, it is easily seen that the possible variations of the Golay-3 array to increase midband contrast are limited due to its simple geometry. The only option would be to increase the sub-aperture diameters, which can only be increased up to the expansion factor before becoming tangent with one another. This would also be undesirable do to an appreciable gain in fill factor and overall size, weight and volume. Therefore, no efforts to increase midband contrast were performed with the Golay-3 array.

3.2 Golay-6 Array

The Golay-6 consists of two sets of three sub-apertures which lie on unique radii from the center of the array, namely R_1 and R_2 , as seen in Figure 6 where the array has an expansion factor of 1.5 [8].

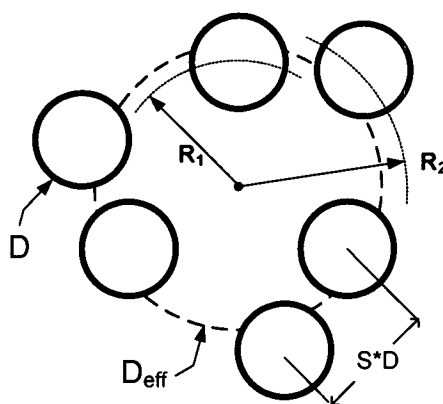


Figure 6: Nominal Golay-6 array.

The same geometry issues of the Golay-3 are seen in the Golay-6 array. If the diameter of any sub-aperture were to be increased they would rapidly become tangent with its closest neighbor. Similarly, if the expansion factor *and* the diameter of a set of sub-apertures

were increased the metrics would become relative in the same manner as the Golay-3 array. Therefore, perturbations to the Golay-6 array will not be explored.

3.3 Golay-9 Array

The Golay-9 array consists of three sets of three sub-apertures that lie on unique radii from the center of the array. The inner-most set of sub-apertures lies on the radius R_1 and the intermediate set and outer-most set lie on the radius R_2 and R_3 , respectively. A nominal diagram of the Golay-9 array with an expansion factor of 1.4 is shown in Figure 7, as this expansion factor has been previously shown to be optimum for the Golay-9 [8].

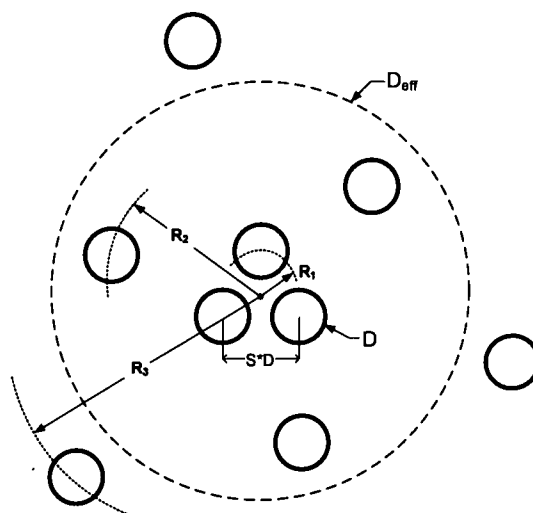


Figure 7: Nominal Golay-9 array

Unlike the Golay-3 and -6, the Golay-9 array has enough degrees of freedom to support change in some of the array's properties. To better understand how to increase mid-frequency contrast, the MTF was observed while sequentially attenuating the different radial sets of sub-apertures, as seen in Figures 8-11. This was done by observing the

MTF while attenuating any given set of sub-apertures and comparing the results to the MTF seen in Figure 8. From this it was determined which sets of sub-apertures were responsible for sampling particular spatial frequency regions. It is important to note that the observed drop-outs in the MTF are the areas of energy corresponding to the attenuated sub-apertures.

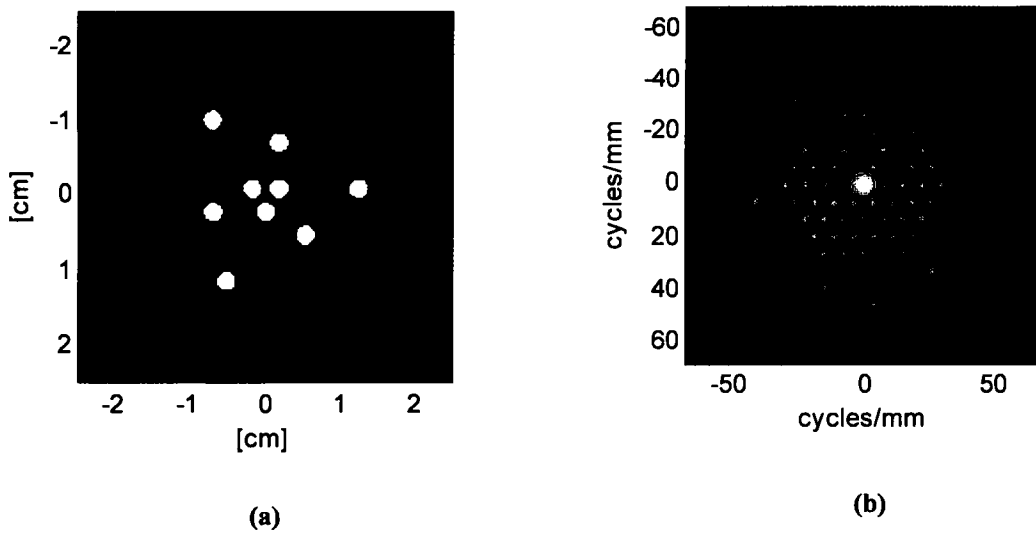


Figure 8: (a) A uniform sub-aperture diameter Golay-9 array with $D=2.54\text{mm}$ and $S=1.4$; and (b) the MTF generated from (a).

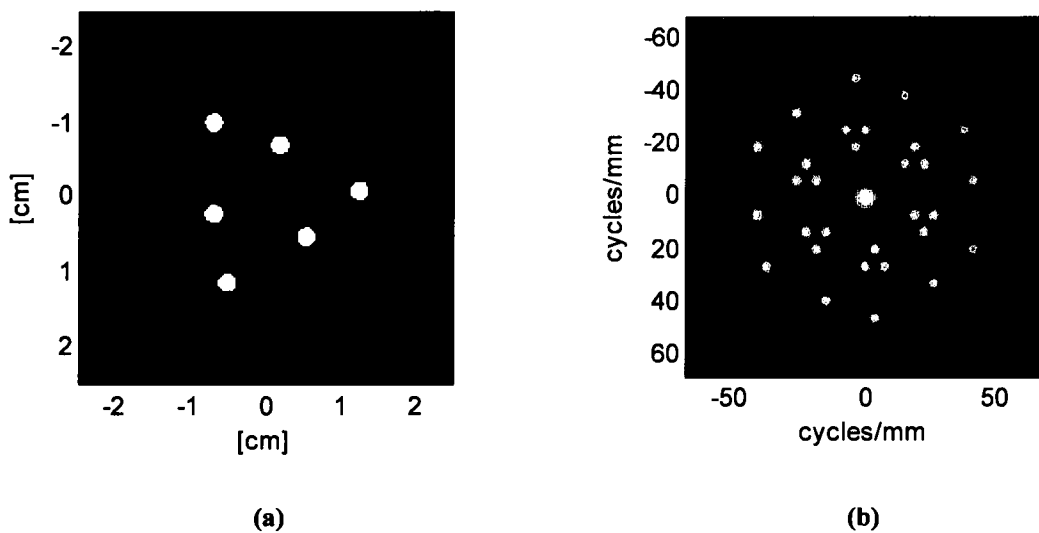


Figure 9: (a) A uniform sub-aperture diameter Golay-9 array with $D=2.54\text{mm}$ and $S=1.4$ with the R_1 set of sub-apertures attenuated by 75%; and (b) the MTF generated from (a).

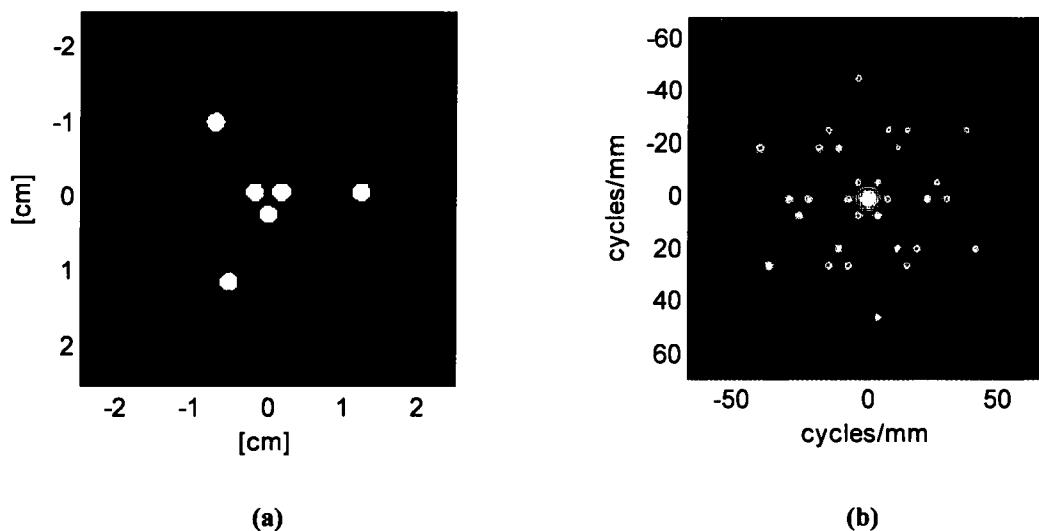


Figure 10: (a) A uniform sub-aperture diameter Golay-9 array with $D=2.54\text{mm}$ and $S=1.4$ with the R_2 set of sub-apertures attenuated by 75%; and (b) the MTF generated from (a).

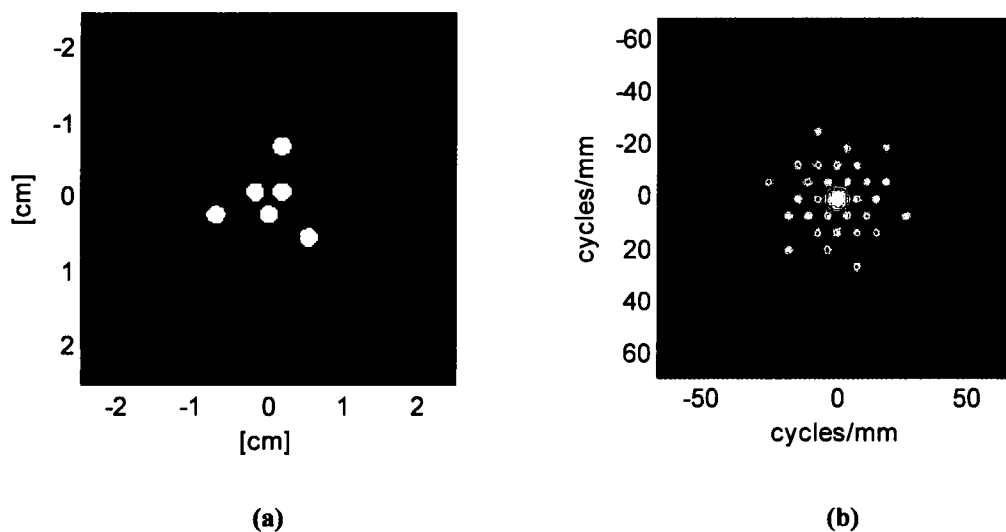


Figure 11: (a) A uniform sub-aperture diameter Golay-9 array with $D=2.54\text{mm}$ and $S=1.4$ with the R_3 set of sub-apertures attenuated by 75%; and (b) the MTF generated from (a).

Figure 8 shows the MTF of an unperturbed uniform sub-aperture diameter Golay-9 array with an expansion factor of 1.4. Then, it is seen in Figure 9 that the R_1 set of sub-apertures is mainly responsible for the low spatial frequency region as well as some mid-

spatial frequency content, but are not responsible for the outlying high spatial frequency content. Also, note that the introduction of autocorrelation redundancy by increasing the diameters of the R_1 set of sub-apertures is unrealistic since their diameters may only be increased up to the expansion factor before becoming tangent. Therefore, the perturbation of the R_1 set of sub-apertures was not explored.

Next, as shown in Figure 10, the R_2 set of sub-apertures is responsible for over 50% of the mid-frequency autocorrelation and exactly 50% of the outlying high spatial frequency content. Furthermore, the R_2 set of sub-apertures are positioned such that there is plenty of room to increase their diameters before overlapping with any other sub-aperture. For these reasons it was chosen to systematically increase the diameters of the R_2 sub-apertures in order to increase autocorrelation redundancy, thereby boosting the MTF at the desired mid-frequencies.

Finally, from Figure 11 it is seen that the R_3 set of sub-apertures is primarily responsible for the outlying, non-contiguous high spatial frequency content. Increasing the diameter of the R_3 set of sub-apertures would therefore not generally be beneficial to increasing the midband contrast. The addition of redundancy would effectively reduce the average relative mid-frequency contrast and therefore the R_3 set of sub-apertures will not be considered for increase in diameter. However, by the same reasoning, as well as the relative nature of MTF levels (i.e. contrast), attenuating the R_3 set of sub-apertures will help to increase the average *relative* contrast at the desired mid-band spatial frequencies.

3.4 Golay-12 Array

Similar to the Golay-9 array, the Golay-12 array has three sets of sub-apertures that lie on unique radii from the center of the array; however, within the intermediate set there are two sets of three sub-apertures, as seen in Figure 12.

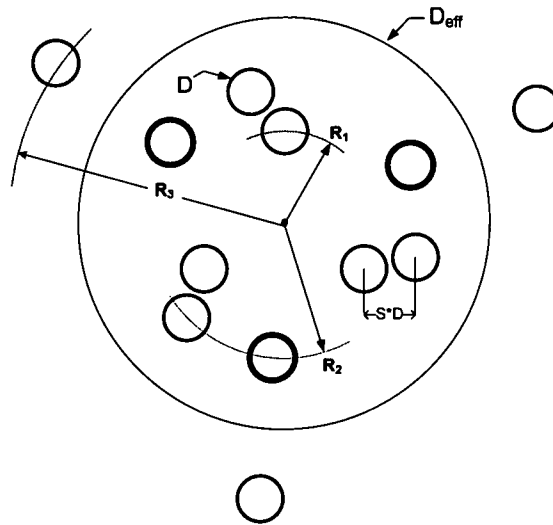


Figure 12: Nominal Golay-12 array.

For notation purposes, the highlighted set of sub-apertures in Figure 12 will be referred to as the R_{21} set of sub-apertures for the Golay-12 array as the non-highlighted set, R_{22} , sub-apertures will remain unchanged.

In a similar fashion to the Golay-9 array, it is observed that the 2-dimensional MTF of the Golay-12 array while sequentially attenuating the different radial sets of sub-apertures. In the Golay-12 array, the R_{22} set of sub-apertures is the set of sub-apertures most closely spaced to the R_1 set of sub-apertures. Intuitively, both of these sets are responsible for the low and mid-spatial frequency MTF energy, as seen in Figures 14 and 15; however, their

diameters cannot be increased because they are the most closely spaced set of sub-apertures. For this reason, any perturbation to these sets of sub-apertures was not explored. Figures 16 and 17 depict the 2-dimensional MTF when the R_{2I} and R_3 sets of sub-apertures are attenuated by 75%, respectively.

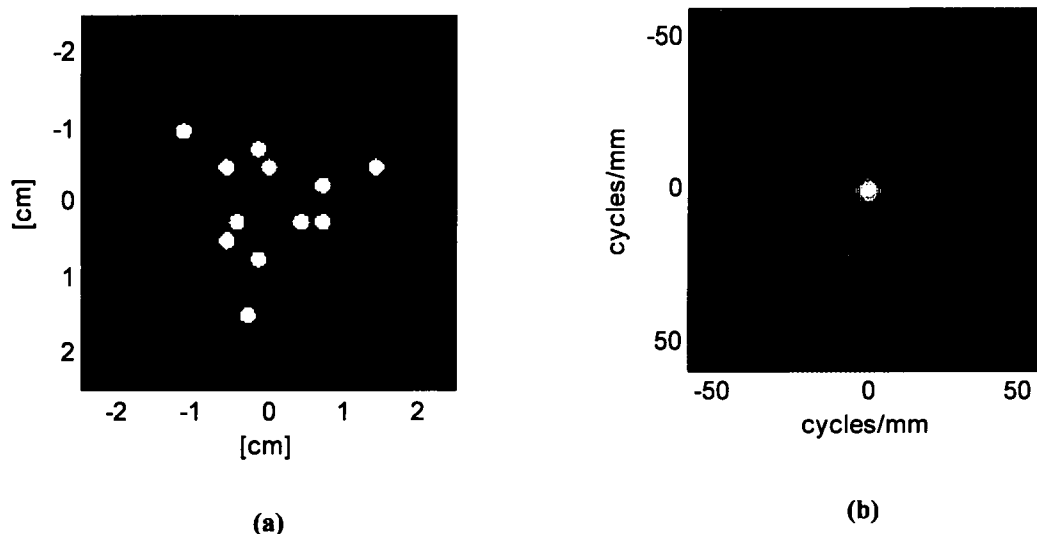


Figure 13: (a) A uniform sub-aperture diameter Golay-12 array with $S=1.3$; and (b) the MTF generated from (a).

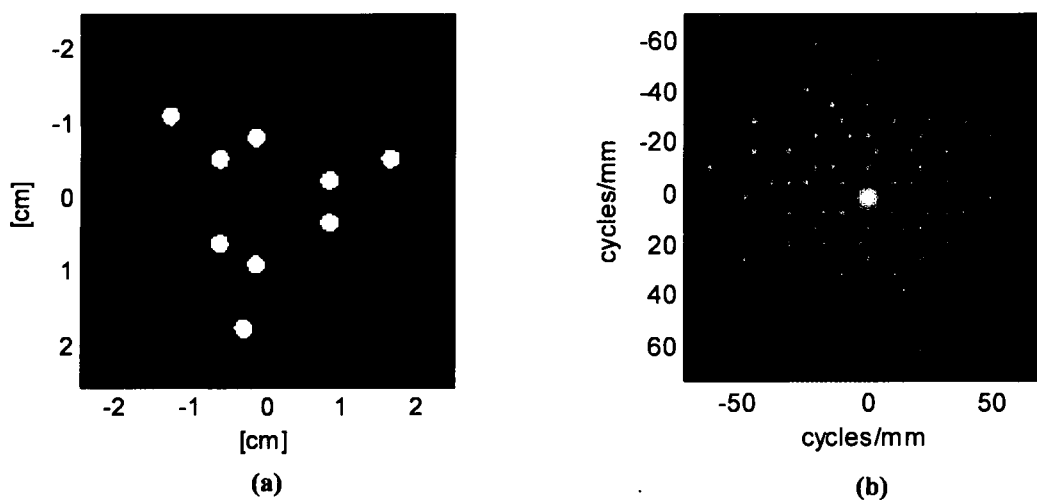


Figure 14: (a) A uniform sub-aperture diameter Golay-12 array with $S=1.3$ and the R_1 set of sub-apertures attenuated by 75%; and (b) the MTF generated from (a).

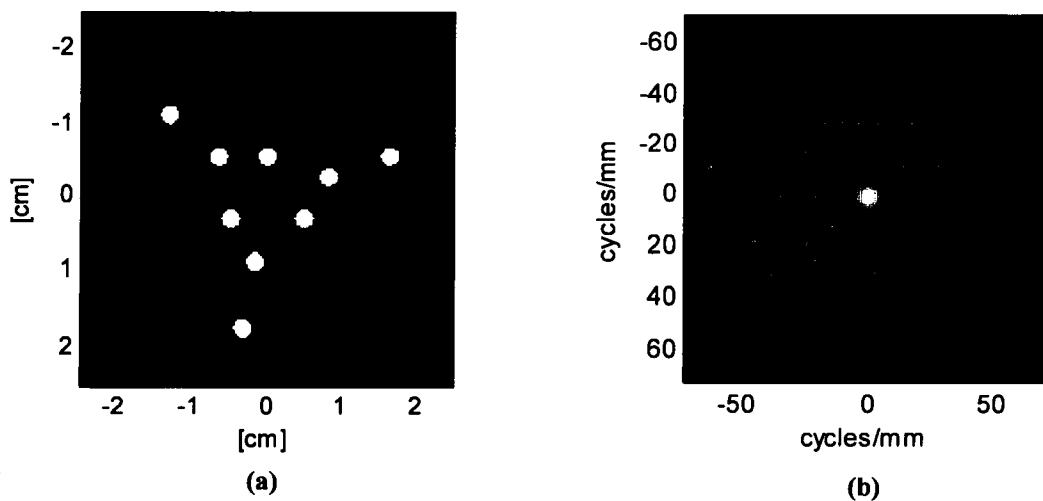


Figure 15: (a) A uniform sub-aperture diameter Golay-12 array with $S=1.3$ and the R_{22} set of sub-apertures attenuated by 75%; and (b) the MTF generated from (a).

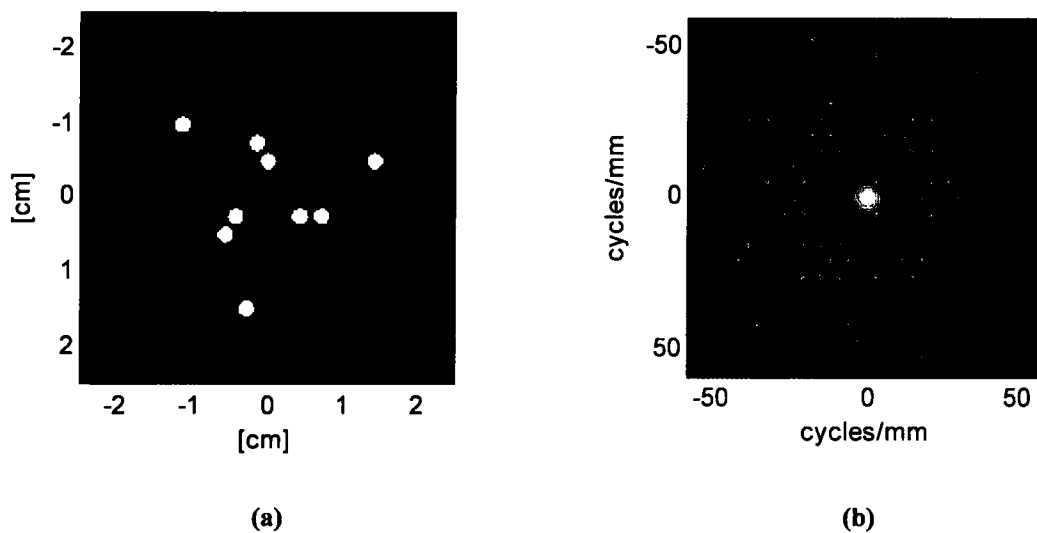


Figure 16: (a) A uniform sub-aperture diameter Golay-12 array with $S=1.3$ and the R_{21} set of sub-apertures attenuated by 75%; and (b) the MTF generated from (a).

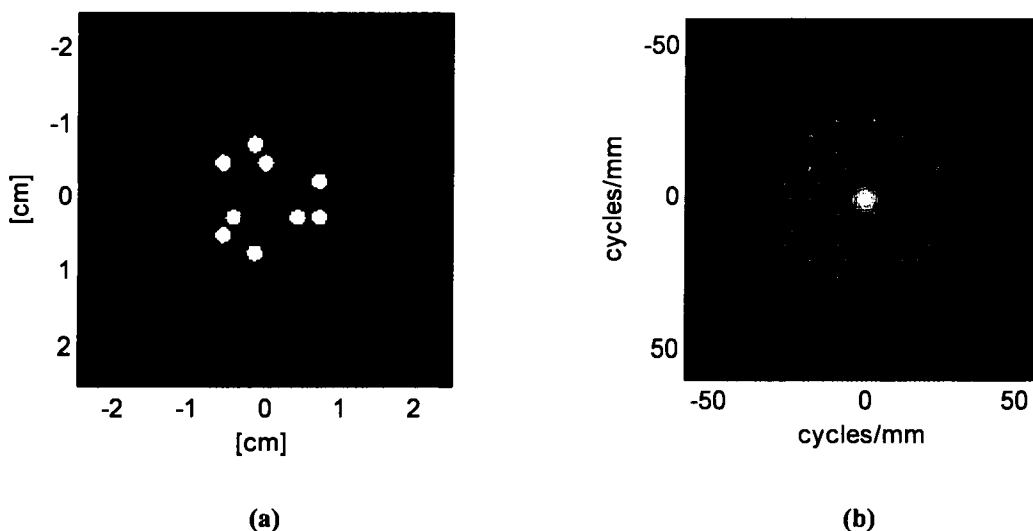


Figure 17: (a) A uniform sub-aperture diameter Golay-12 array with $S=1.3$ and the R_3 set of sub-apertures attenuated by 75%; and **(b)** the MTF generated from (a).

Figure 13 shows an unperturbed uniform sub-aperture diameter Golay-12 array with an expansion factor of 1.3. Then it is seen in Figure 16 that the R_{21} set of sub-apertures is mainly responsible for mid-spatial frequency content as well as less than 50% of the outlying high spatial frequency content. Therefore, it was elected to enlarge their diameters in order to increase midband autocorrelation at the desired midband spatial frequencies. Note also that the geometry of the Golay-12 array allows for such increases.

It is seen in Figure 17 that the R_3 set of sub-apertures is mainly responsible for the high spatial frequency content, specifically all of the outlying, non-contiguous high spatial frequency region. Again, due to the relative nature of the ARC metric attenuation effects of the R_3 set of sub-apertures will be investigated.

CHAPTER 4

SPATIAL FREQUENCY AVAILABILITY TECHNIQUE

Previously the most conservative approach in defining the spatial frequency cutoff ρ_{min} was taken by using the diameter of the largest circle which could be inscribed within the contiguous portion of the MTF, which correlates to finding the first radial zero. An example of the conservative spatial frequency cutoff is shown in Figure 18 for uniform diameter Golay-9 and -12 arrays with expansion factors of 1.4 and 1.3, respectively.

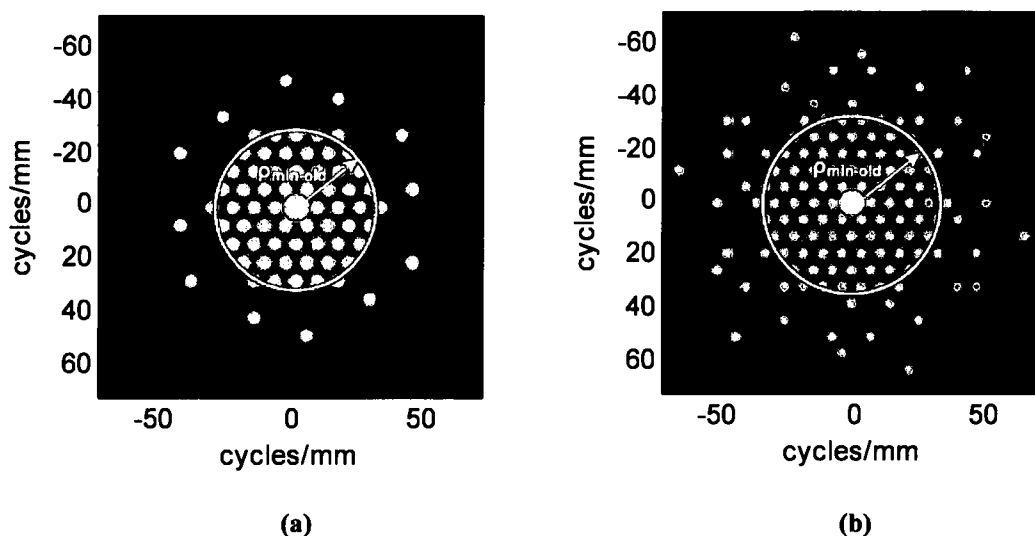


Figure 18: The MTF of (a) a Golay-9 array with $D=2.54\text{mm}$ and $S=1.4$; and (b) a Golay-12 array with $D=2.54\text{mm}$ and $S=1.3$. The spatial frequency cutoff, determined by the conservative maximum inscribed circle approach, is shown by the white circle.

4.1 Calculating the Spatial Frequency Cutoff

It was found that efforts to increase mid-frequency contrast by increasing the diameter of the R_2 or R_{2I} sub-apertures can make the contiguous portion of the MTF start to overlap with what was previously outlying high spatial frequency content, as seen in Figures 19 and 20. This effect gives rise to reduced gaps in the MTF, causing the spatial frequency cutoff to be poorly described using previous methods. Therefore, a new algorithm was developed, consistent with the conventional approach, which fairly incorporates some of the new energy introduced into the MTF as D_{R2} (or D_{R2I}) increases relative to D_{R1} and D_{R3} .

The growth of a binary Golay-9 MTF is shown below in Figures 19 and 20 for R_2 sub-aperture diameters ranging from unity to 2.8. It is important to note the differences between growth in Figure 19 (a) and (b), where there is still an obvious contiguous portion, compared to the difference between Figure 20 (a) and (b), where there is not an obvious contiguous portion and there are deep nulls in the radial spatial frequency. The new spatial frequency availability technique is useful in that the asymmetries introduced by the substantially increased autocorrelation redundancy will create MTF energy outside the previous contiguous portion, which would be otherwise neglected using the previous method of finding spatial frequency cutoff, as seen in Figure 20 (b).

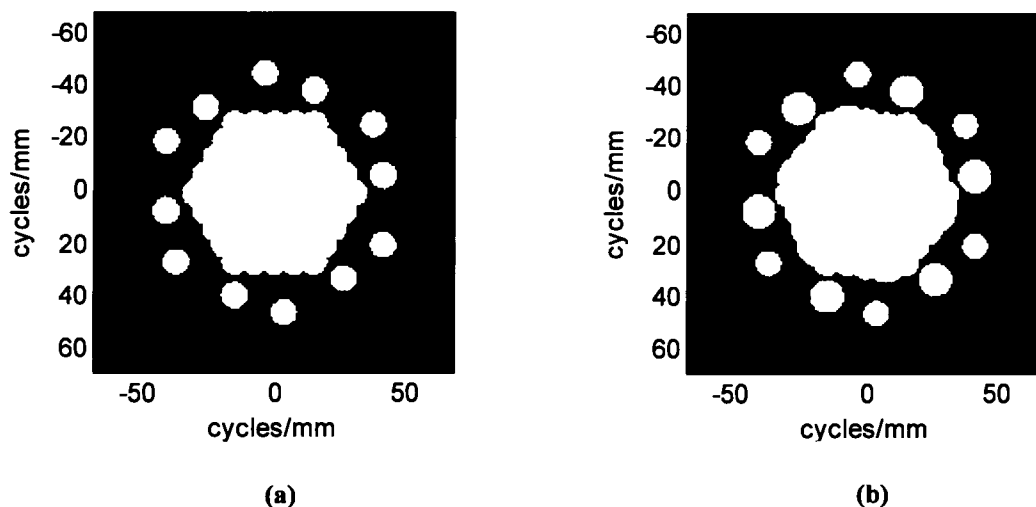


Figure 19: The binary MTF of a Golay-9 array with $S=1.4$ and (a) uniform sub-aperture diameters; and (b) the R_2 sub-aperture diameter increased to 1.6 times the unit diameter.

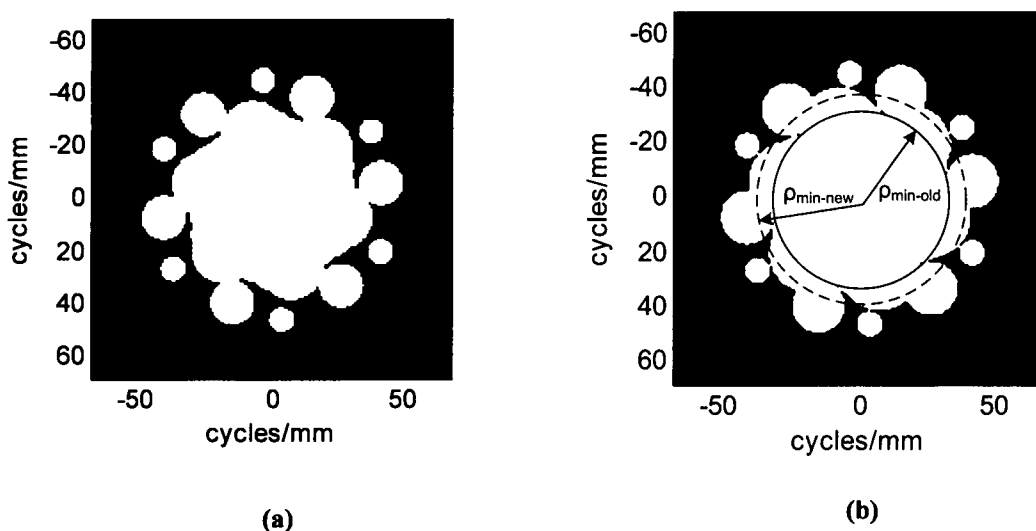


Figure 20: The binary MTF of a Golay-9 array with $S=1.4$ and (a) the R_2 sub-aperture diameter increased to 2.2 times the unit diameter; and (b) the R_2 sub-aperture diameter increased to 2.8 times the unit diameter.

The new spatial frequency cutoff algorithm is based on an imaging system's ability to successfully image radial spatial frequencies. It has come to be called the "spatial frequency availability" algorithm. This algorithm is implemented by first setting a threshold T_l for acceptable optical power in the midband spatial frequencies, and then

creating a binary version of the MTF as shown, for example, in Figure 19 (a) for $T_1=0$. For practical imaging systems T_1 would be set according to the minimum acceptable SNR level within the midband of the MTF.

The fractional open areas of a series of thin concentric annuli (each about 0.01 cyc/mm when $D=1\text{mm}$) are then calculated to determine the availability of particular radial spatial frequencies, after which a second threshold T_2 is chosen. This second threshold specifies the minimum fraction of any given radial spatial frequency that must be available in the final image. Setting a high threshold ($T_2 \approx 1$) will yield the previously used conservative approach to defining spatial frequency cutoff, and would reduce to choosing the radius of the largest circle inscribed within the contiguous portion of the MTF, as shown in Figure 20 (b).

4.2 Calculating the Midband Average Relative Contrast (ARC)

A mid-frequency optical power metric was then defined to compare the average midband contrast of various Golay-9 arrays to that of a fully filled aperture with the same effective diameter. In order to consider only midband contrast improvement, the optical power present in the center lobe of the MTF (with uniform sub-aperture diameters) as well as all optical power outside ρ_{min} , as determined according to the new algorithm has been neglected. Specifically, the midband average relative contrast (ARC) is defined as the integrated midband optical power of a sparse array, normalized with respect to the integrated midband optical power of a resolution equivalent fully-filled aperture according to the following relationship:

$$ARC = \frac{\int_0^{2\pi} \int_{\frac{D}{\lambda s_i}}^{\rho_{\min}} MTF_{sparse}(\rho, \phi) \rho d\rho d\phi}{2\pi \int_{\frac{D}{\lambda s_i}}^{\rho_{\min}} MTF_{fully-filled}(\rho) \rho d\rho}, \quad (7)$$

where

$$MTF_{fully-filled} = \begin{cases} \frac{2}{\pi} \left[\arccos\left(\frac{\rho}{\rho_{\min}}\right) - \frac{\rho}{\rho_{\min}} \sqrt{1 - \left(\frac{\rho}{\rho_{\min}}\right)^2} \right] & \rho \leq \rho_{\min} \\ 0 & \text{otherwise,} \end{cases} \quad (8)$$

and MTF_{sparse} is the MTF of the sparse aperture imaging system and is found by taking the modulus of Equation (4) or (6). Note that the denominator in Equation (7) is symmetric in ϕ and therefore the angular integral is simply 2π . The ARC metric has proven useful in that it allows us to quantitatively describe and compare various Golay patterns for optical performance.

CHAPTER 5

INCREASING MIDBAND CONTRAST IN GOLAY-LIKE ARRAYS

5.1 Introduction of Redundancy

As determined in Chapter 3, enlarging the diameters of the R_2 and R_{2l} set of sub-apertures in the Golay-9 and -12 array, respectively, can increase autocorrelation redundancy at the desired midband spatial frequencies. Sections 5.1.1 and 5.1.2 will present the numerical expectations.

5.1.1 Golay-9 Array

Numerical calculations of spatial frequency cutoff, fill factor and ARC were performed for several R_2 sub-aperture diameters using various T_l and T_2 values. In all cases the positions of the sub-apertures were fixed to that of the uniform sub-aperture diameter Golay-9 array, with an expansion factor of 1.4. The R_1 and R_3 sets of sub-apertures were set to 2.54mm and the distance from the pupil plane to the image plane was taken to be one focal length. The diameters of the R_2 set of sub-apertures were then increased. Plots for $T_l=0$ and $T_l=0.01$, with $T_2=0.98$ and $T_2=0.90$, are provided in Figures 21-24. Setting $T_l=0$ corresponds to the perfect, noiseless case, while the $T_l=0.01$ threshold was chosen by examining the noise level in the experimental setup. In particular, T_l was chosen to be very small while also allowing as many detector noise-induced artifacts as possible to be

removed from the MTFs created from measured data. Corresponding to the experimental conditions described in the Chapter 6, a focal length of 750mm was assumed and the source wavelength was set to 632.8nm.

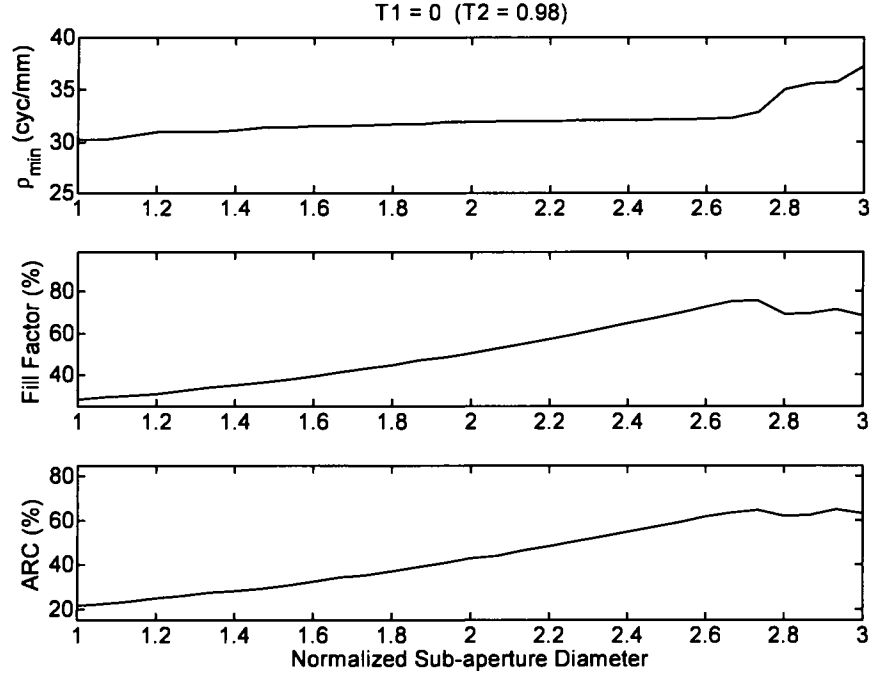


Figure 21: Numerical simulations of spatial frequency cutoff ρ_{min} , fill factor α and midband average relative contrast (ARC) for varying D_{R2} with an initial threshold of $T_1=0$ and spatial frequency availability threshold of $T_2=0.98$.

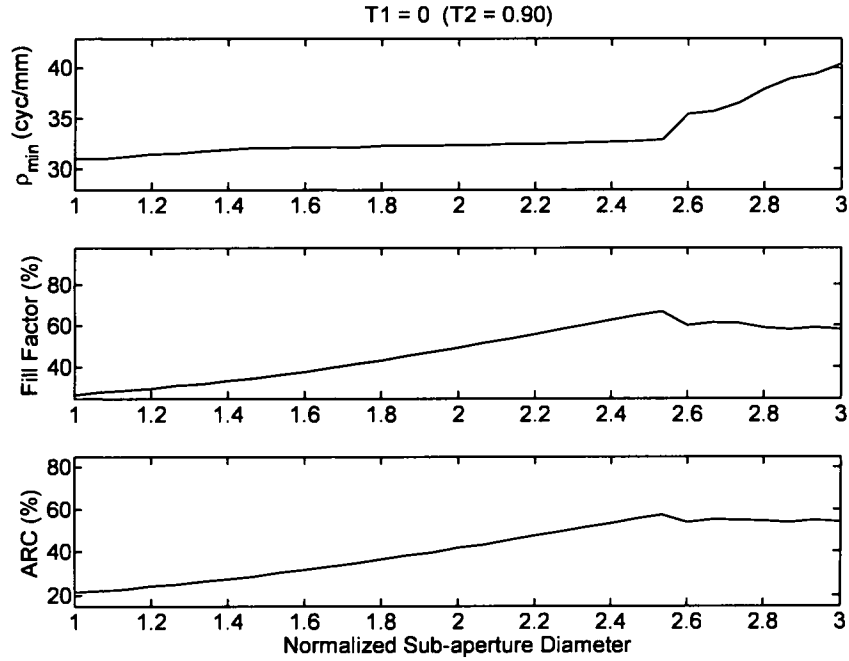


Figure 22: Numerical simulations of spatial frequency cutoff ρ_{min} , fill factor α and midband average relative contrast (ARC) for varying D_{R2} with an initial threshold of $T_1=0$ and spatial frequency availability threshold of $T_2=0.90$.

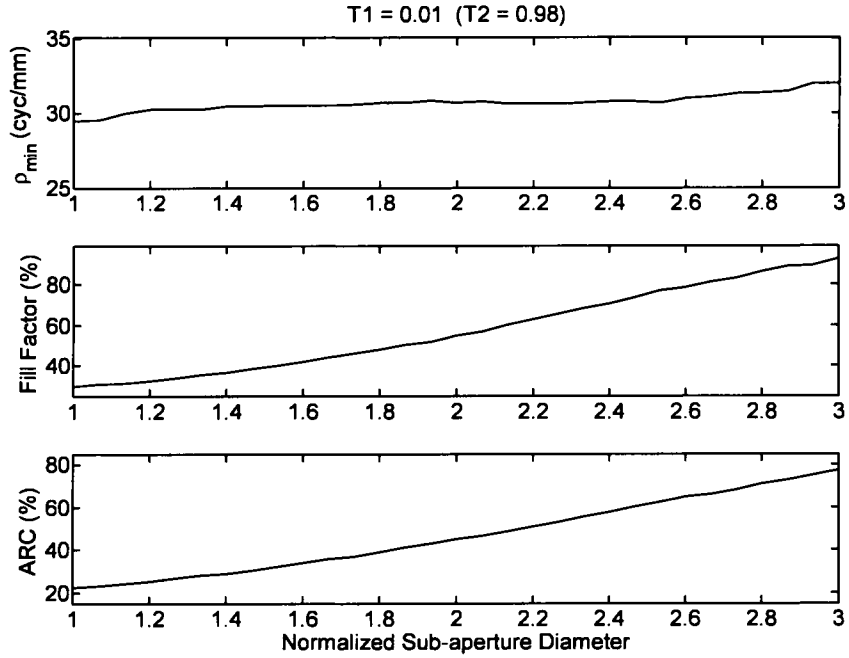


Figure 23: Numerical simulations of spatial frequency cutoff ρ_{min} , fill factor α and midband average relative contrast (ARC) for varying D_{R2} with an initial threshold of $T_1=0.01$ and spatial frequency availability threshold of $T_2=0.98$.

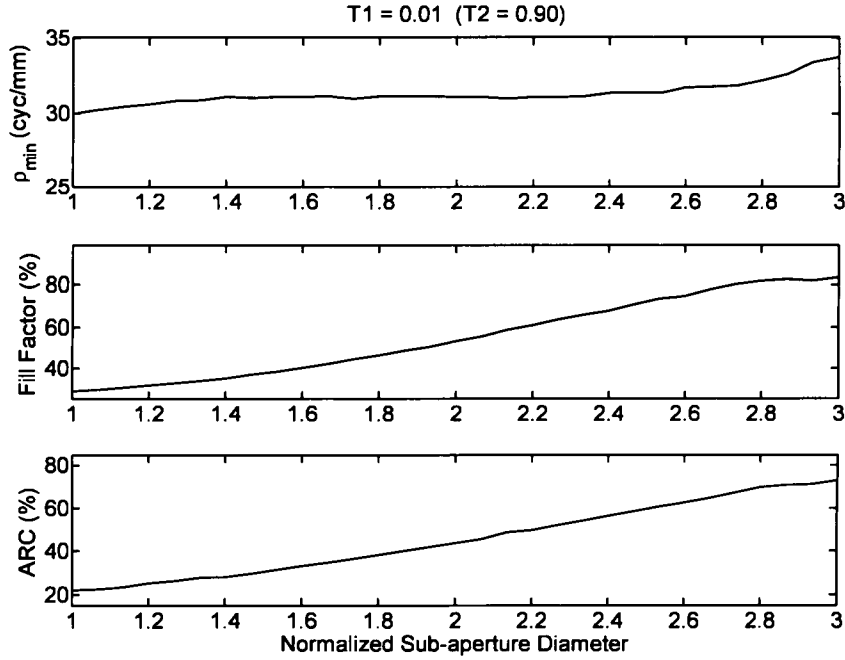


Figure 24: Numerical simulations of spatial frequency cutoff ρ_{min} , fill factor α and midband average relative contrast (ARC) for varying D_{R2} with an initial threshold of $T_I=0.01$ and spatial frequency availability threshold of $T_2=0.90$.

As shown in Figures 21-24, for small increases in the R_2 sub-aperture diameters a slight increase in spatial frequency cutoff is observed. An appreciable increase in the average relative midband contrast is also seen while maintaining a relatively sparse fill-factor while achieving a maximum ARC increase of 55%. Notice in Figures 21 and 22 that there is a sudden increase in ρ_{min} when the relative diameter of the R_2 set of sub-apertures reaches ~ 2.7 . It is believed that this is an anomaly of the noiseless case and arises from the significant overlap of the contiguous portion of the MTF with what was previously outlying high spatial frequency content. As the SNR threshold (T_I) increases a more realistic sampling of the MTF occurs and this effect is much less severe, as seen in Figures 23 and 24.

5.1.2 Golay-12 Array

Numerical calculations for the Golay-12 array were performed in the same manner as in the previous section for the Golay-9 array. Plots for $T_1=0$ and $T_1=0.01$, with $T_2=0.98$ and $T_2=0.90$ are provided in Figures 25-28.

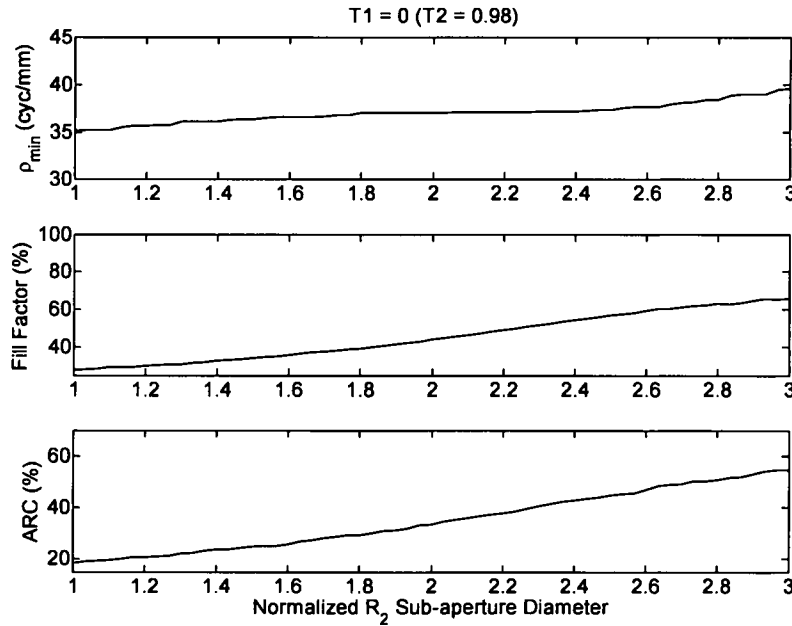


Figure 25: Numerical simulations of spatial frequency cutoff ρ_{min} , fill factor α and midband average relative contrast (ARC) for varying D_{R21} with an initial threshold of $T_1=0$ and spatial frequency availability threshold of $T_2=0.98$.

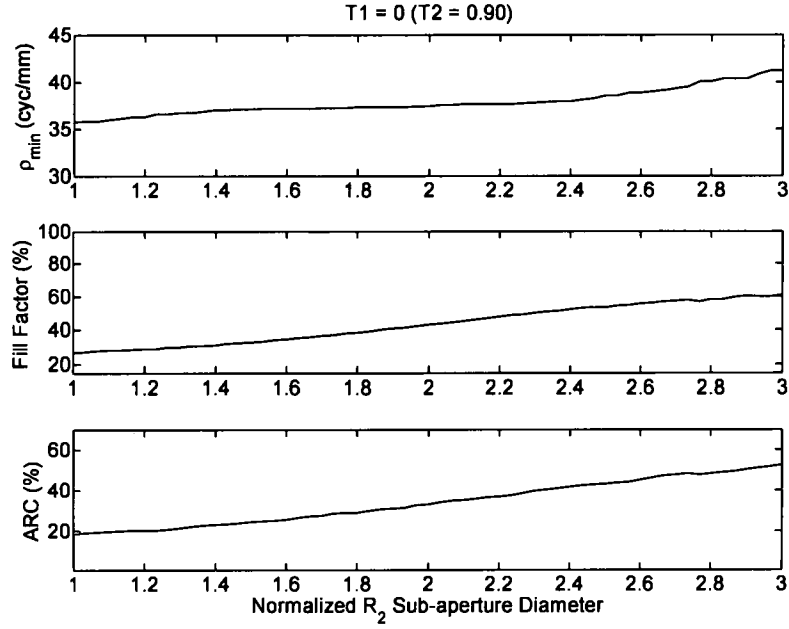


Figure 26: Numerical simulations of spatial frequency cutoff ρ_{min} , fill factor α and midband average relative contrast (ARC) for varying D_{R2I} with an initial threshold of $T_I=0$ and spatial frequency availability threshold of $T_2=0.90$.

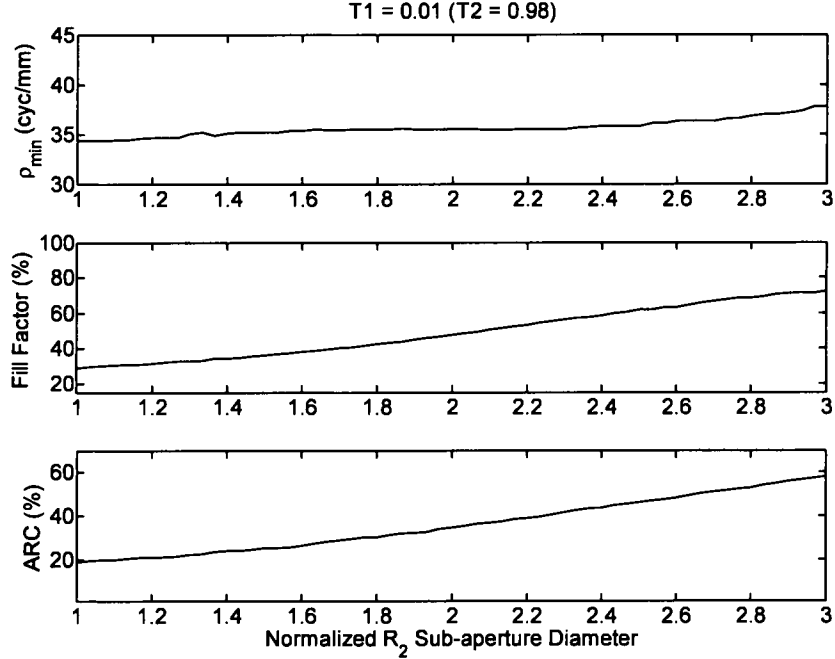


Figure 27: Numerical simulations of spatial frequency cutoff ρ_{min} , fill factor α and midband average relative contrast (ARC) for varying D_{R2I} with an initial threshold of $T_I=0.01$ and spatial frequency availability threshold of $T_2=0.98$.

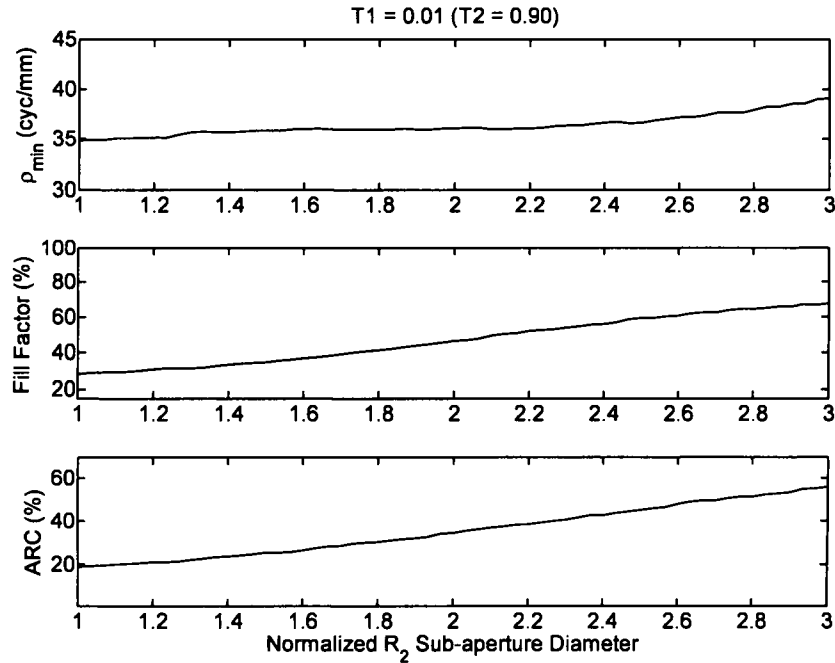


Figure 28: Numerical simulations of spatial frequency cutoff ρ_{min} , fill factor α and midband average relative contrast (ARC) for varying D_{R2I} with an initial threshold of $T_I=0.01$ and spatial frequency availability threshold of $T_2=0.90$.

The results presented in Figures 25-28 follow the same trends as in the Golay-9 numerical simulations. The introduction of autocorrelation redundancy in the Golay-12 array yields a slight gain in resolution and an increase of 37% in midband average relative contrast. The fill factor remains slightly lower for substantial increases in diameter of the R_{2I} set of sub-apertures as compared to the Golay-9 array, but the maximum midband contrast recovery is 20% less.

The Golay-12 array requires larger increases in the R_{2I} sub-aperture diameters (and therefore fill factor) to achieve increases in ARC comparable to the Golay-9. For example, to achieve an ARC value of 35.4% in the Golay-12 array, the diameter of the R_{2I} set of sub-apertures has to be increased to 2.033 times the uniform diameter. This

correlates to a fill factor of 47%. A Golay-9 array with the same fill factor (47%) can achieve an ARC value of 39.4%, which is better than the Golay-12 with the same fill factor. This occurs when the diameter of the R_2 set of sub-apertures have a diameter of only 1.833 times the unit diameter. Note that these results are consistent with previous research concluding that the Golay-12 array is beyond the point of diminishing returns [8].

5.2 Discrete Global Apodization Effects, Attenuation

It was determined in Chapter 3 that attenuating the R_3 set of sub-apertures could boost the midband contrast due to the relative nature of the metrics. The proceeding sections will discuss and present numerical expectations of these attenuation effects.

5.2.1 Golay-9 Array

The opacity of the R_3 set of sub-apertures was varied from 50% to 100% transmissive and the average relative midband contrast was computed. The effect of R_3 sub-aperture attenuation is seen in Figures 29 and 30 for the same scenario as seen in Figure 21 (i.e. $T_1=0$, $T_2=0.98$). Figure 29 is for uniform sub-aperture diameters and Figure 30 is for the case where the diameters of the R_2 set of sub-apertures are 2.73 times the unit diameter, which is where the maximum ARC value occurred for numerical simulations, as seen in Figure 21.

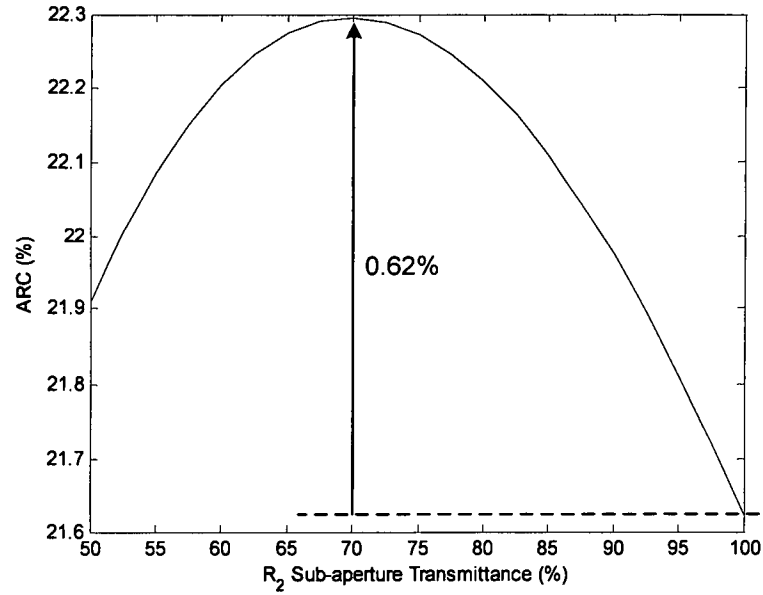


Figure 29: Numerical simulations of midband average relative contrast (ARC) while attenuating the R_3 set of sub-apertures in the uniform sub-aperture diameter Golay-9 array from 50% transmittance to 100% transmittance.

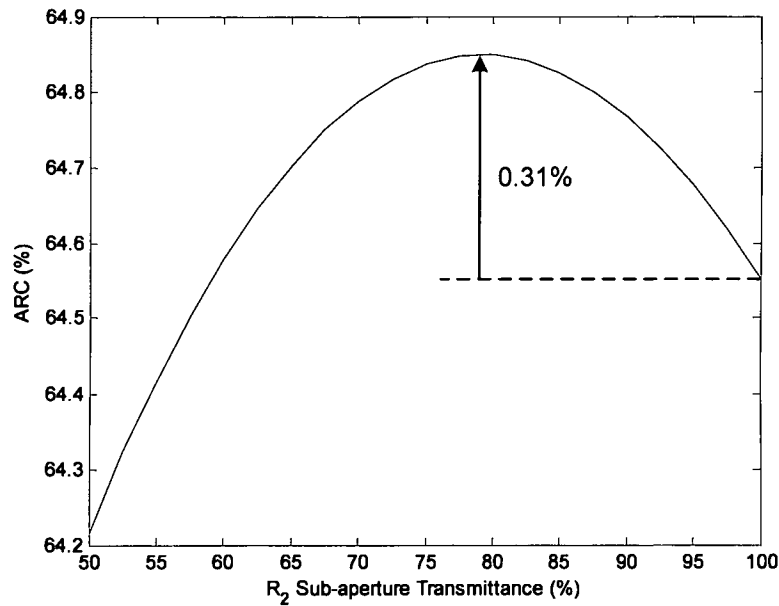


Figure 30: Numerical simulations of midband average relative contrast (ARC) while attenuating the R_3 set of sub-apertures in the Golay-9 array with a R_2 sub-aperture diameter of 2.73 times the unit diameter from 50% transmittance to 100% transmittance.

Attenuating the R_3 set of sub-apertures increased the relative mid-frequency contrast; however, it is a marginal effect compared to the introduction of redundancy. Figure 29 shows only a 0.62% increase in midband contrast when the R_3 set of sub-aperture's transmission is reduced to $\sim 70\%$. Figure 30 shows only a 0.31% increase in midband contrast when the R_3 set of sub-aperture's transmission is reduced to $\sim 79\%$.

These attenuation effects are dependent on the diameter of the R_2 set of sub-apertures. Furthermore, this effect was most influential with *smaller* R_2 sub-aperture diameters (i.e. uniform sub-aperture diameters as seen in Figure 29) making this effect most practical for arrays with little or no introduction of redundancy in the R_2 set of sub-apertures. It should also be noted that the greatest amount of attenuation required to obtain maximum ARC is for the unit sub-aperture case.

5.2.2 Golay-12 Array

Numerical calculations were performed for the attenuation of the R_3 set of sub-apertures in the Golay-12 array in the same manner as in section 5.2.1. The effect of R_3 sub-aperture attenuation is presented in Figures 31 and 32 for the same scenario as seen in Figure 19 (i.e. $T_1=0$, $T_2=0.98$). Figure 31 is for uniform sub-aperture diameters and Figure 32 is for a R_{21} sub-aperture diameter of 2.73. This R_{21} sub-aperture diameter was chosen because there is no local maximum in the ARC calculations for the Golay-12 and the following data can then be easily compared to the Golay-9 calculations.

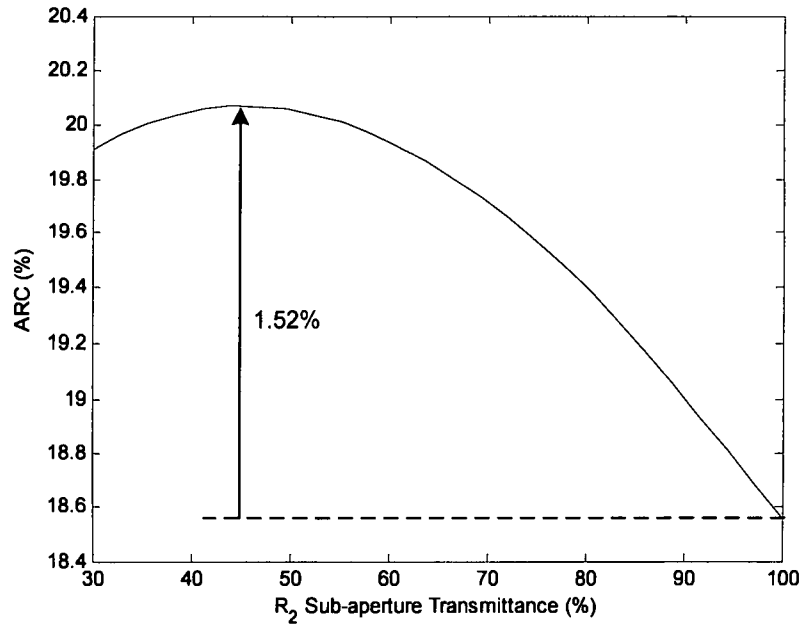


Figure 31: Numerical simulations of midband average relative contrast (ARC) while attenuating the R_3 set of sub-apertures in the uniform sub-aperture diameter Golay-12 array from 30% transmittance to 100% transmittance.

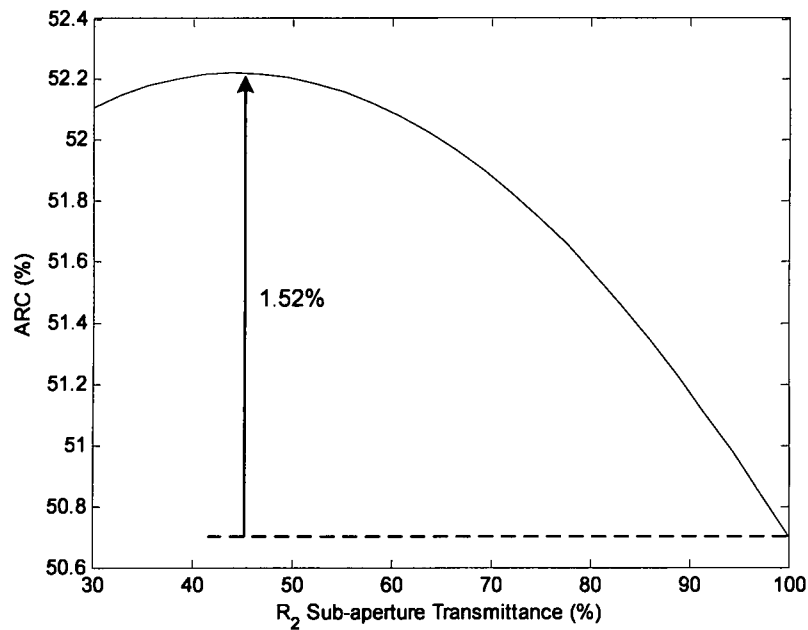


Figure 32: Numerical simulations of midband average relative contrast (ARC) while attenuating the R_3 set of sub-apertures in the Golay-9 array with a R_{21} sub-aperture diameter of 2.8 times the unit diameter from 50% transmittance to 100% transmittance.

As in the Golay-9 case, the attenuation of the R_3 set of sub-apertures marginally increased the relative midband contrast. It is seen in figures 31 and 32 that the maximum ARC value occurred when the R_3 set of sub-apertures was attenuated by 55%, for both the uniform sub-aperture diameter and the enlarged R_2 sub-aperture cases. A maximum ARC increase of 1.52% was seen in both of these cases, which is a slightly larger increase than seen in the Golay-9 array.

It is important to note that, unlike in the Golay-9, the attenuation effects in the Golay-12 are not dependant on moderate increases in the diameter of the R_{2l} set of sub-apertures. This can be attributed to the large amount of outlying high spatial frequency content in the MTF generated from the Golay-12 array as compared to the MTF generated from the Golay-9 array. As shown in Chapter 3, this outlying high spatial frequency content is generated from the correlation of a R_3 sub-aperture with another sub-aperture in the array. Then, as the MTF is a normalized function, the increase in ARC via attenuating the R_3 set of sub-apertures remains a larger effect when the diameter of the R_{2l} set of sub-apertures is increased than as seen in the Golay-9 array.

CHAPTER 6

EXPERIMENTAL VERIFICATION OF THEORY

6.1 Experimental Setup

Figure 33 shows a diagram of the experimental setup. Multiple Golay-9 masks with varying R_2 sub-aperture diameters were placed before an imaging lens L_2 . The masks were then illuminated with a spatially filtered and collimated laser source having a wavelength of $\lambda=632.8\text{nm}$. Both lenses L_1 and L_2 were well corrected three inch diameter doublets having focal lengths of 750mm. In order to magnify the PSF and allow better spatial sampling, a microscope objective was placed one focal length after the imaging lens. The magnified intensity PSF was then recorded by the CCD array. Finally, after scaling the measured PSF dimensions by the system magnification, for each value of D_{R2} the MTF was found by taking the modulus of the OTF calculated by use of Equation (4).

The magnification factor for the system was measured by comparing the pixel distance between three sets of distinct outer lobes in the theoretical, unmagnified PSF, and the experimental, magnified PSF. See, for example, the white arrowed lines of Figure 34. Using the average experimental center-to-center pixel spacing between the three sets of distinct lobes, taken over three experimental PSF realizations, the magnification factor was found to be 3.63.

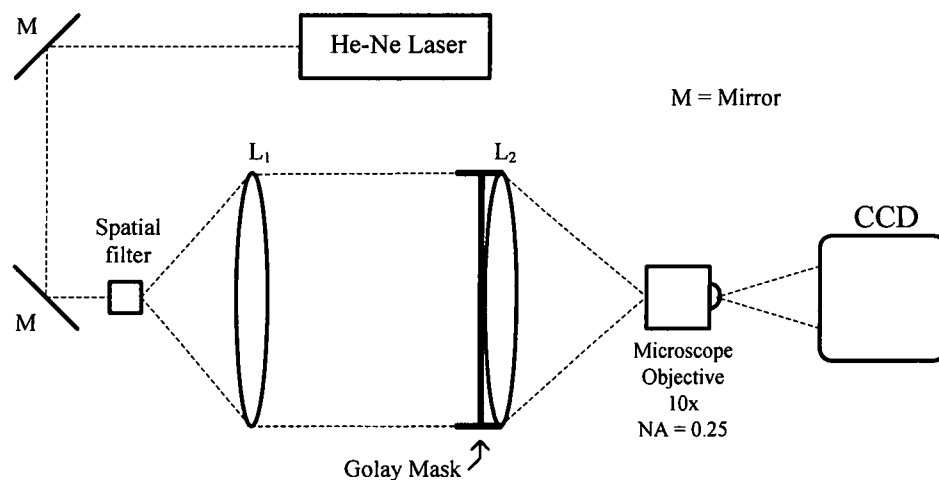


Figure 33: Diagram of the experimental setup.

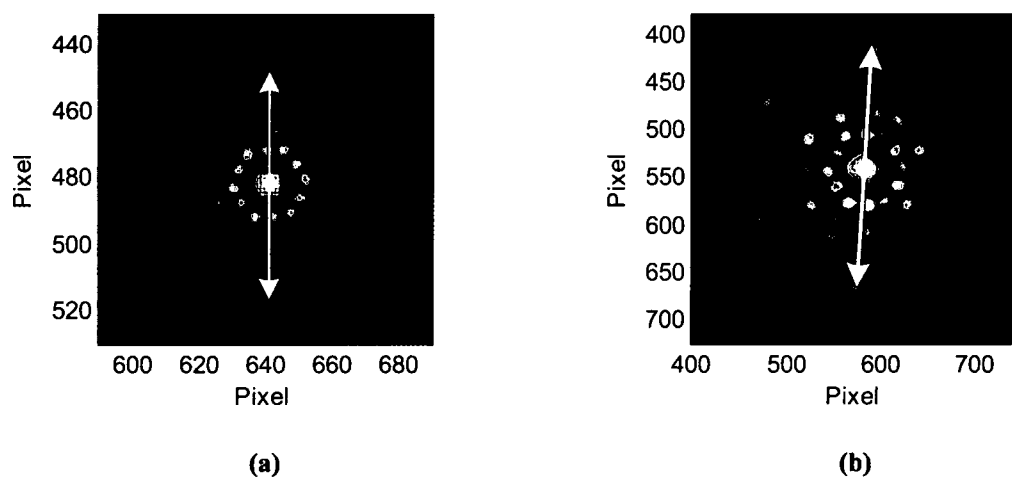


Figure 34: An example of one set of distinct lobes for which the center-to-center pixel spacing was recorded in (a) the theoretical, unmagnified PSF; and (b) an experimental, magnified PSF.

6.2 Results

The MTF and associated metrics were calculated (assuming $T_1 = 0.01$ and $T_2 = 0.98$) for a uniform diameter ($D = 2.54$ mm) Golay-9 mask, as well as for four other Golay-9

masks whose R_2 sub-aperture diameters were increased by factors of 1.7, 2.0, 2.4 and 2.8. The theoretical expectations are plotted in Figure 35 along with the values determined from experimental data.

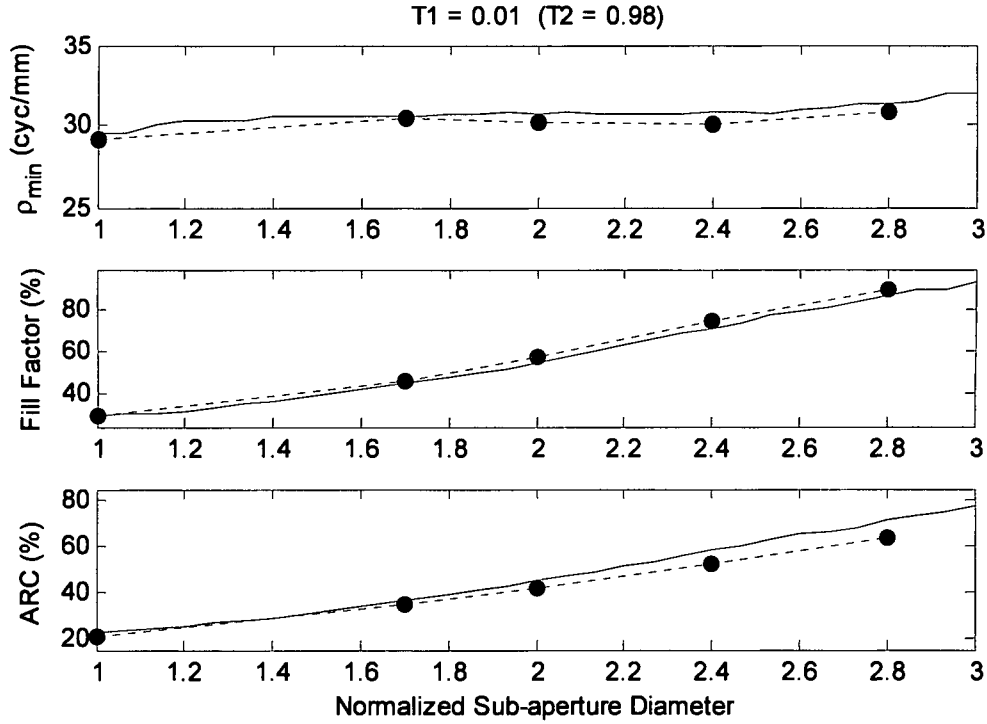


Figure 35: Theoretical (solid) and experimental (dashed) calculations of spatial frequency cutoff p_{min} , fill factor α and midband average relative contrast (ARC) using an initial threshold of $T_1=0.01$ and a spatial frequency availability threshold of $T_2=0.98$.

It is believed that the experimental results presented in Figure 35 match the theoretical expectations very well. Notice, though, that the experimentally determined spatial frequency cutoffs are consistently a bit smaller than theory predicts. This intuitively produces higher fill factors and lower ARC values according to Equations (1) and (7). Though not shown here, the same set of data was also analyzed for several other spatial frequency availability thresholds T_2 . In all cases, the data followed the theory in the same manner shown in Figure 35.

CHAPTER 7

SUMMARY AND CONCLUSIONS

Sparse aperture imaging is a useful technique for obtaining high resolution images while maintaining a small light collection area with respect to a large, resolution-equivalent monolithic aperture. However, conventional sparse aperture systems suffer from reduced midband contrast.

A new method for determining spatial frequency cutoffs for sparse aperture arrays having semi-redundant autocorrelations was developed based upon the notion of radial spatial frequency availability. The quantitative average relative contrast metric was then developed in order to describe the recovery of mid-frequency contrast as sparse array autocorrelation redundancy is increased. From these metrics we were able to compare perturbed versions of the nominal Golay-9 and -12 arrays to their resolution equivalent monolithic apertures.

In particular, numerical simulations were performed to examine the midband contrast recovery caused by increasing the diameter of the intermediate radius set of sub-apertures in a Golay-9 array. An increase in average relative contrast of over 55% can be achieved, but at the expense of an increased fill factor. These numerical expectations were then experimentally verified with very little disagreement observed between theory and data.

Therefore, it is concluded that for modest increases in the diameters of the R_2 set of sub-apertures the midband contrast of a Golay-9 array can be enhanced, while suffering only marginal increases in array fill factor.

Numerical simulations were also performed for the Golay-12 array. An increase in average relative contrast of over 35% can be achieved, but again at the expense of an increased fill factor. As for the Golay-9 array, the midband contrast of a Golay-12 array can be enhanced, while suffering only marginal increases in array fill factor.

Also observed were the effects of attenuating the R_3 set of sub-apertures in both the Golay-9 and -12 arrays. Although, in theory, there was an optimum opacity of the R_3 set of sub-apertures which increased the midband relative contrast, it was only a marginal effect, especially compared to the appreciable gains seen by the introduction of redundancy.

Moreover, the spatial frequency cutoff algorithm and the average relative contrast metric can be extended to describe the performance of any sparse aperture imaging system. As the results will scale with wavelength, sub-aperture diameter and system magnification it is believed that the techniques will be useful to other researchers examining a wide variety of other sparse aperture imaging systems.

REFERENCES

- [1] J.S. Fender, "Synthetic apertures: an overview," Proc. SPIE **440**, 2-7 (1983).
- [2] S. -J. Chung, D. W. Miller and O. L. Weck, "Design and implementation of sparse aperture imaging systems," Proc. SPIE **4849**, 181-192 (2002).
- [3] J. E. Harvey, A. Kotha and R. L. Phillips, "Image characteristics in applications utilizing dilute subaperture arrays," Applied Optics **34**, 2983-2992 (1995).
- [4] R. D. Flete, T. A. Tantaló, J. R. Calus and J. A. Mooney, "Image quality of sparse-aperture designs for remote sensing," Opt. Eng. **41**(8), 1957-1969 (2002).
- [5] M. J. Golay, "Point arrays having compact, nonredundant autocorrelations," J. Opt. Soc. Am. **61**, 272-273 (1971).
- [6] J. R. Fienup, "MTF and integration time versus fill factor for sparse-aperture imaging systems," Proc. SPIE **4091**, 43-47 (2000).
- [7] J. R. Fienup, "Comparison of reconstruction algorithms for images from sparse-aperture systems," Proc. SPIE **4792**, 1-8 (2002).
- [8] N. J. Miller, M. P. Dierking and B. D. Duncan, "Optical sparse aperture imaging," Appl. Opt. **46** 5933-5943 (2007).
- [9] J. W. Goodman, *Introduction to Fourier Optics*, 3rd ed., (Roberts and Company, Englewood, CO, 2005), Chapt. 6.
- [10] Q. Wu, L. Qian and W. Shen, "Configuration optimization of a kind of sparse-aperture system," Proc. SPIE **6024**, 602420 (2005).

R002594778